Modelling of Inertial Fusion and High Energy Density Physics Targets with HYDRA

M. M. Marinak

Lawrence Livermore National Laboratory

Presented at the

Workshop on Computational Challenges in Hot Dense Plasmas

Institute for Pure and Applied Mathematics,

University of California, Los Angeles

March 30, 2012

LLNL-PRES-543472

This work was performed under the auspices of the U.S. Department of Energy by Lawrence Livermore National Security, LLC, Lawrence Livermore National Laboratory under Contract DE-AC52-07NA27344

Acknowledgements:

G. Kerbel, B. Chang, M. Patel, S. Sepke, J. Koning, N. Gentile

Design of ICF experiments and interpretation of results requires codes which treat a full spectrum of processes

- HYDRA is a 2D/3D parallel multiphysics ICF simulation code
  - has been in use for 18 years.
- HYDRA models the physics necessary for simulations of ICF and NIF ignition
  - A wide range of models for physical processes available for designer to choose
  - Broad variety of model ingredients supported for EOS, opacities, conductivities, …
  - Highly flexible zoning, with multiblock mesh allows mesh to conform to the target as needed
- HYDRA has been extensively tested against data on NIF, Omega, Nova, Titan, with a long list of results published in refereed journals

HYDRA is applied to simulate a wide variety of targets by users at various institutions

- Development of HYDRA is a collaborative effort between LLNL and SNL
- HYDRA is used at SNL, Rochester LLE, LANL, LBNL and various universities
- HYDRA is applied to a wide variety of targets including:
  - Indirect drive capsules only simulations of NIF, Omega, Nova experiments
  - Direct drive capsule only simulations
  - Integrated hohlraum simulations (ignition, symcaps, re-emission, shock timing)
  - Heavy ion ignition target designs, Warm Dense Matter experiments
  - Z-pinches
  - Theta pinch (Xe studies for LIFE)
  - Fast ignition integrated target design
  - Planar Rayleigh-Taylor targets
  - Direct drive jet formation experiments
  - ...

In the National Ignition Campaign the most common uses include

- Preshot simulations guide design of experiments
- Postshot calculations analyze experiment as realized
- Capsule only simulations can include roughness on all surfaces fill tube, isolated defects, ice cracks
  - Over large solid angle 2D/3D
  - Very high resolution 2D/3D simulations over wedge up to $\ell \sim 2000$
  - Studies of Be crystalline structure

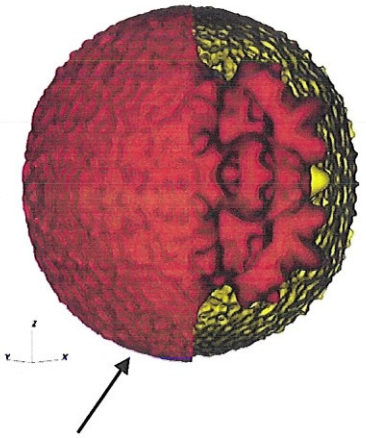

RT and RM instabilities are principally important

ICF capsules are subject to ablative and density gradient stabilization

Therefore only a limited range of modes is RT unstable

This makes practical direct numerical simulations resolving essentially the full range of unstable modes

RT perturbation growth is limited to weakly nonlinear regime

Zoning requirements for resolving RT and RM have been quantified, facilitating numerically converged simulations

$$\Gamma = \sqrt{\frac{\alpha g k}{1 + k L_n}} - \beta k V_a$$

In the National Ignition Campaign the most common uses include (cont.)

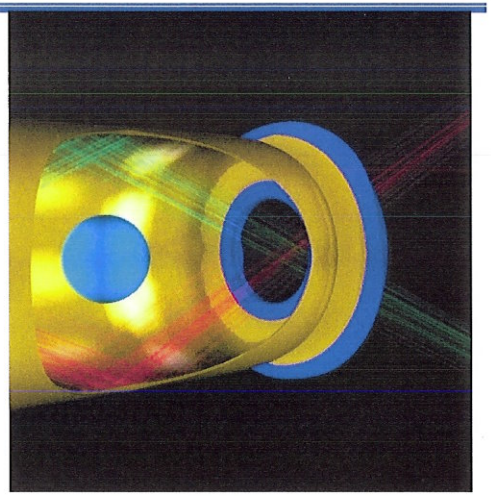

- Integrated hohlraum simulation
  - Ignition hohlraums, THD
  - Symmetry capsule
  - Re-emission sphere
  - Shock timing "keyhole"
  - 3D including intrinsic and extrinsic drive asymmetry, patches in targets, cones
  - Recent 2D high resolution integrated simulations resolve surface roughness up to $\ell \sim 100$

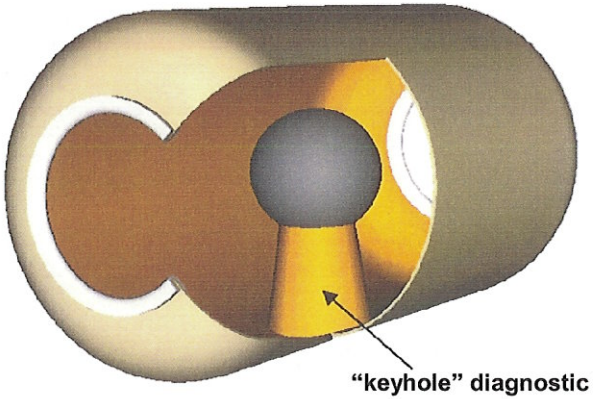

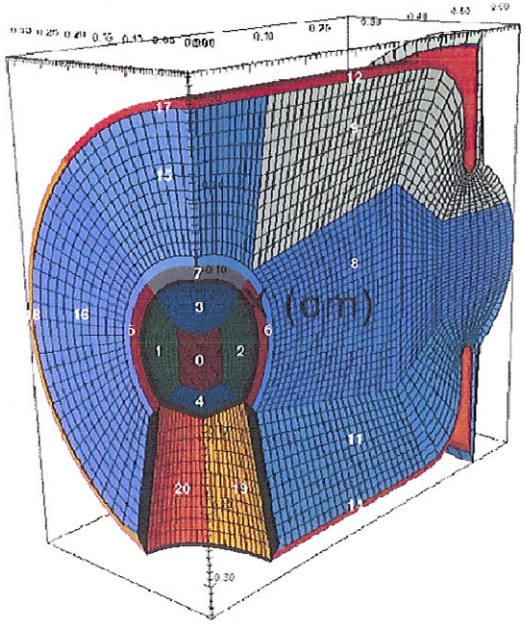

Physical processes modeled by the HYDRA code for ICF simulations

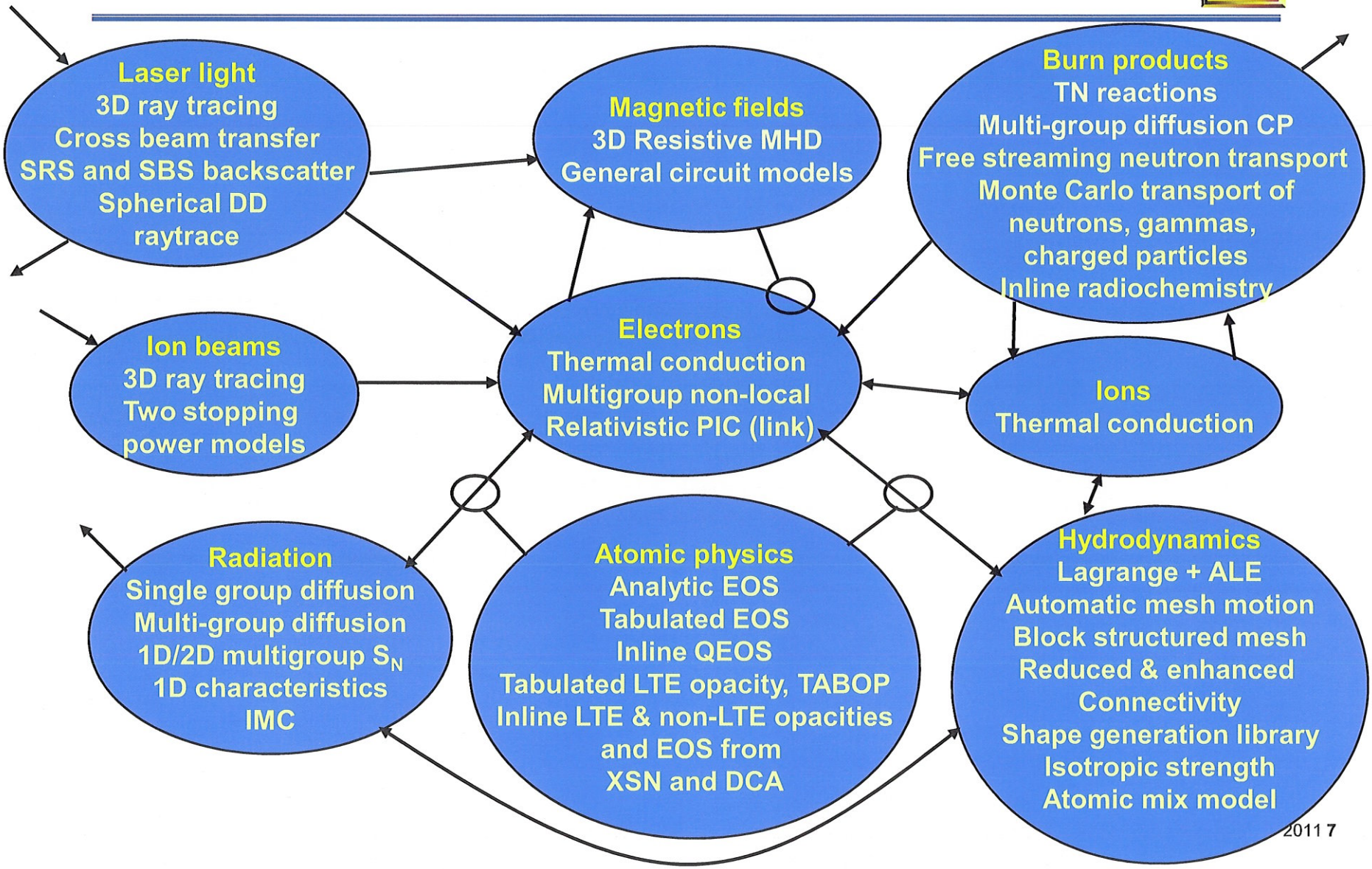

ICF requires high density physics models

- Fermi-degenerate electron effects on
  - Pressure and energy
  - Electron conduction
  - Atomic physics
  - Charged particle stopping

- Pressure ionization and continuum lowering effect
  - Pressure and energy
  - Opacity, especially at low $h\nu$

Regions of pressure ionization and degeneracy in hydrogen EOS

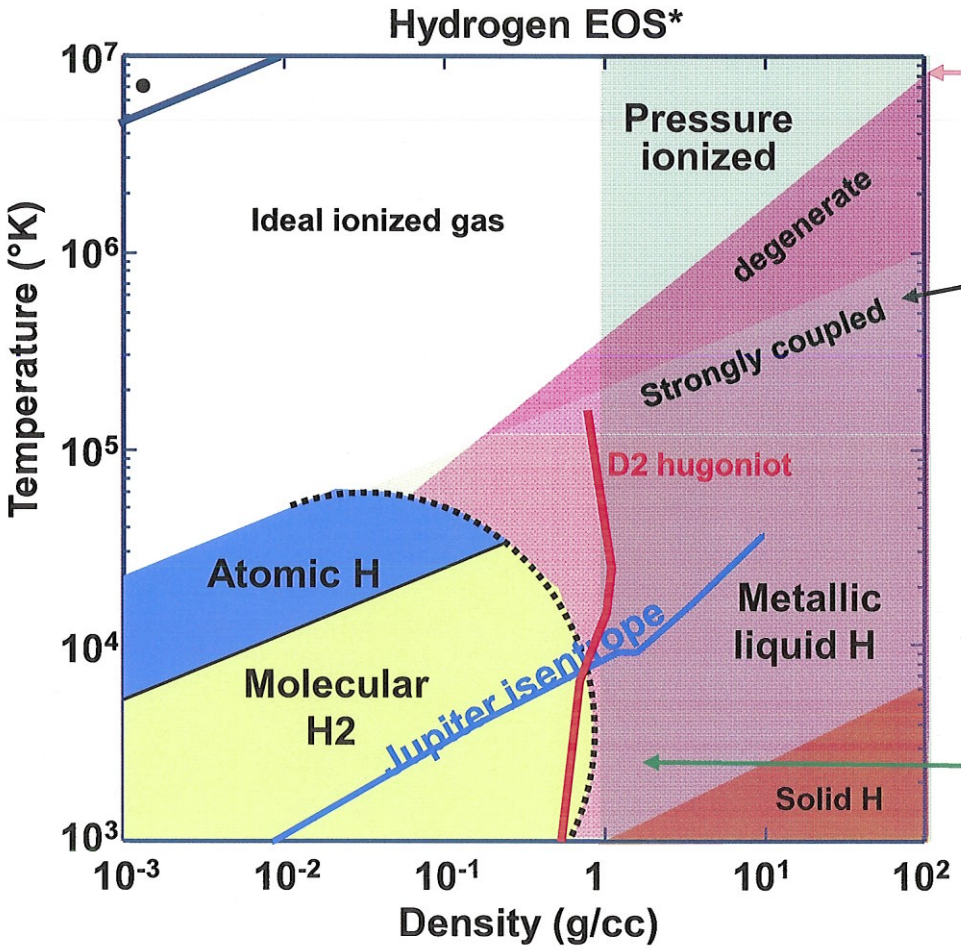

Degeneracy
- kT ~ E (Fermi) = $p^2/2m_e$,
- Particle correlations become important

Strongly coupled plasmas

$$\Gamma \equiv \frac{Z^2 e^2 / a}{kT} = \frac{Coulomb}{Thermal}$$

$$\propto Z^{5/6} n_e^{1/3} / T$$

- Long range correlations become important

Pressure ionization
- Bohr radius ~ inter-ion spacing
- Ionization potentials are depressed

VanHorn, Science, 252(1991)

Atomic data obtained from many sources

Tabulated opacities and equations-of-state (EOS) are available for LTE problems

Tabulated EOS can be mixed and/or scaled by a Thomas-Fermi model

An inline EOS package QEOS:

- Handles all materials (time-dependent mix)
- Maintains exact thermodynamic consistency
- Provides smooth data for hydro-instability calculations

Inline atomic kinetics packages XSN and DCA

- Can provide LTE and non-LTE opacities, emissivities and EOS
- Evolve equations for level populations dynamically

laser raytrace

Laser propagation and deposition are treated using a ray tracing model

- 3D laser raytrace
- Refraction calculation based upon piecewise linear electron density
- Inverse Bremsstrahlung absorption includes screening and intensity-dependent effects
- Ponderomotive force
- Smearing technique smooths zonal energy deposition
- Scattering surfaces with parameterized models (Harvey-Shack)
- Special raytrace model for DD spherical implosions (HYDRA)
- Working on implementing a low noise model for polar DD spherical implosions using 3D raytrace in HYDRA (with LLE)

Thermal electron transport is an important heat flow process in many targets

- Electron thermal conduction is usually modeled with flux-limited diffusion
- Diffusion operator is finite finite element
  - HYDRA supports degenerate elements
- Electron conductivity is affected by:
  - Fermi degeneracy, partial ionization, magnetic fields, collective effects
- Nonlocal model in HYDRA retains main features of kinetic effects through convolution of Spitzer-Harm flux with delocalization kernel[1]
  - We have extended the method to enable implicit time stepping
  - Recently added multigroup cascade of hot electrons
- Transport of relativistic hot electrons modelled running HYDRA in conjunction with Zuma relativistic PIC code
  - Integrated simulations of fast ignition targets

1. G. P. Schurtz, P. D. Nicolai, and M. Busquet, Phys. Plasmas **7**, 4238 (2000)

radiation

Choice of several radiation transport methods enables QA and accuracy/speed tradeoffs

- Implicit Monte Carlo – workhorse for integrated hohlraum calculations in HYDRA
- Multigroup diffusion – Used for "low noise" hydro instability / weakly anisotropic radiation flux
- Single-group diffusion (LTE only)
- S_N multigroup transport
  - New Polar S_N under development in HYDRA

radiation

ICF/HED simulations require multigroup treatment of radiation transport equations

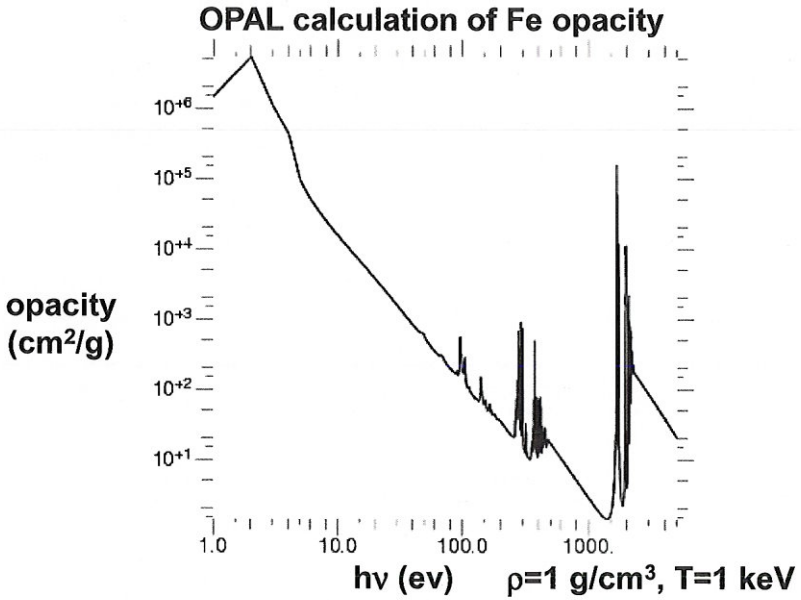

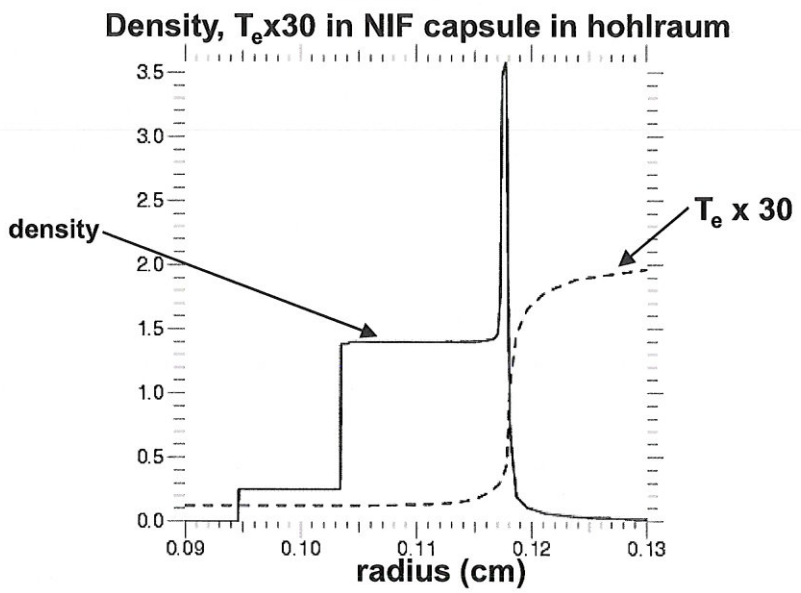

- Frequency-resolved radiation transport required to obtain correct ablation rate, ablation velocity (= $\dot{m}/\rho$), density gradient scale length.
- These quantities all affect Rayleigh-Taylor and Richtmyer-Meshkov instability growth. Preheat from high energy photons affects material ahead of ablation front.

Nonlocal thermodynamic equilibrium treatment often necessary

- When collisional processes dominate the atomic excitation rates - occupation probabilities agree with thermodynamic equilibrium irrespective of radiation intensities.
- When radiative processes begin to dominate, such as at low collisionality or high radiation intensity, non-LTE (NLTE) required
- Solve for I_ν and atomic "populations"

$$\rho \frac{D\left(N_{ij}/\rho\right)}{Dt} = \sum_k \left[N_{ik}\left(R_{kj}+C_{kj}\right) - N_{ij}\left(R_{jk}+C_{jk}\right)\right]$$

- R's are radiative rates (i.e. spontaneous and stimulated decay, photoabsorption, photoionization), C's are collisional rates

$$\frac{1}{c}\frac{\partial I_\nu}{\partial t} + \hat{\Omega}\cdot\vec{\nabla} I_\nu = j_\nu - k_\nu I_\nu$$

solve simultaneously

J. Castor, *Radiation Hydrodynamics*, Cambridge University Press, 2004; D. Salzmann, Atomic Physics in Hot Plasmas, Oxford, 1998

Recent enhancements have enabled gold hohlraum modeling with DCA

Code-to-code comparisons for Au ionization level from NLTE-4 (2005) & NLTE-5 (2007) workshops

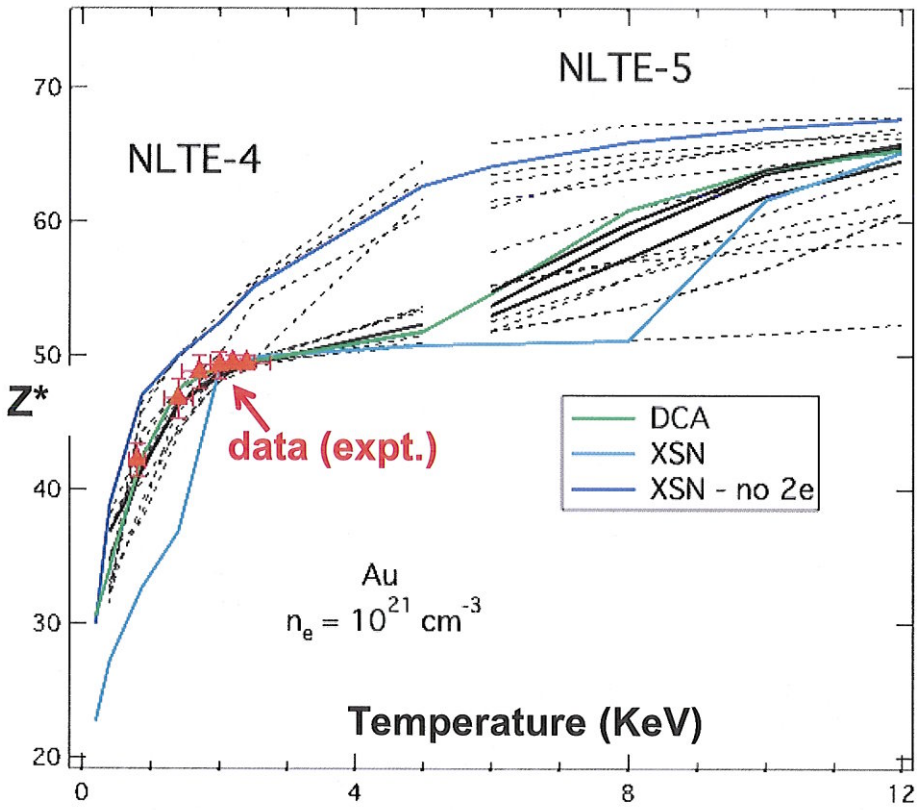

DCA (CRETIN) exhibits good agreement with other codes over a large range of T_e

Term splitting and configuration broadening of photoexcitations [1]

- Photoexcitations are split into multiple term-to-term transitions with individual energies and oscillator strengths

  e.g. n=2 → n=3 becomes

  2p- → 3s+,2s+ → 3p-, 2s+ → 3p+,

  2p- → 3d-, 2p+ → 3d-, 2p+ → 3d+,…

DCA agrees with more detailed models and is fast enough for in-line use

[1] H. A. Scott, S.B. Hansen, Advances in NLTE modeling for integrated simulations, High Energy Density Phys. 6, 39-47 (2010).

Measured Dante flux is in good agreement with pre-shot simulations using HYDRA-DCA

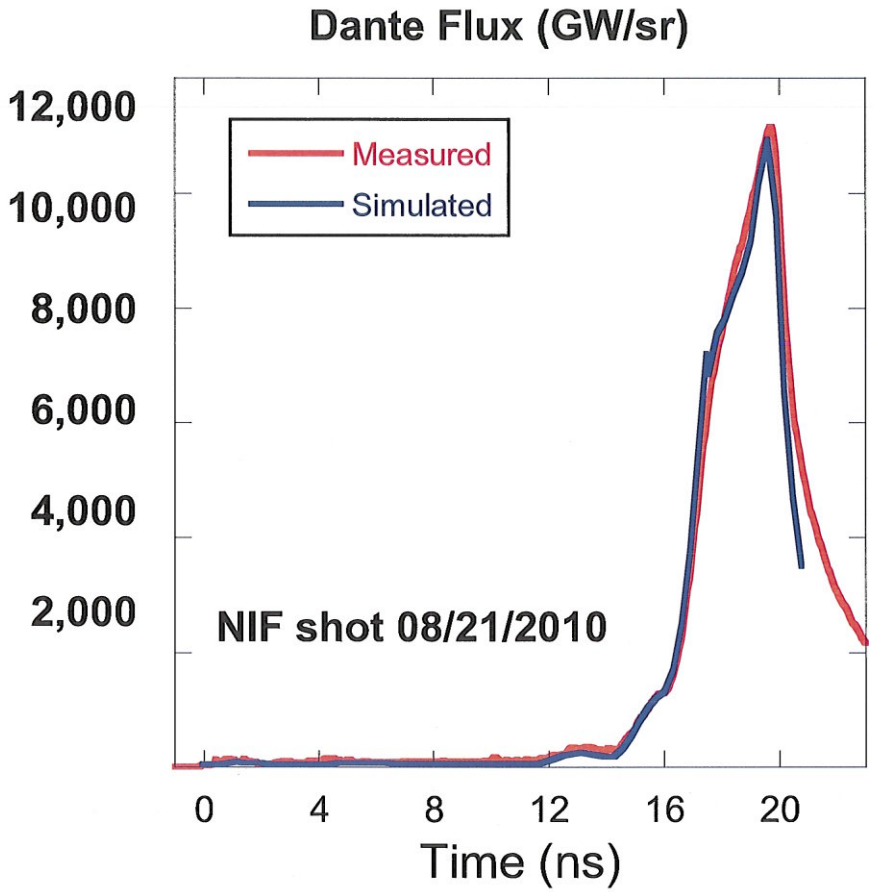

Measured = 1MJ symmetry capsule expt. (8/21/2010)

Simulated = pre-shot HYDRA-DCA with non-local electron transport (N. Meezan, LLNL)

This pre-shot calculation used a flat-in-time SRS (t) profile. Post-shot simulations use the measured SRS (t) profiles.

DCA model for gold employed had ~1300 levels, ~49000 photoexcitation transitions, ~3100 photoionization transitions, ~4300 collisional excitation transitions

Hydrodynamic instability and high compression calculations challenge numerical methods

- Lagrangian hydrodynamics on 2D quadrilateral or 3D hexahedral well suited for large spherical compressions

- Any numerical noise that arises is amplified by hydrodynamic instabilities, such at Rayleigh-Taylor and Richtmyer-Meshkov
  - Differentiability of algorithms should be considered

An experiment on Nova examined growth of a prescribed 3-D multimode perturbation on a foil

Radiograph of sample

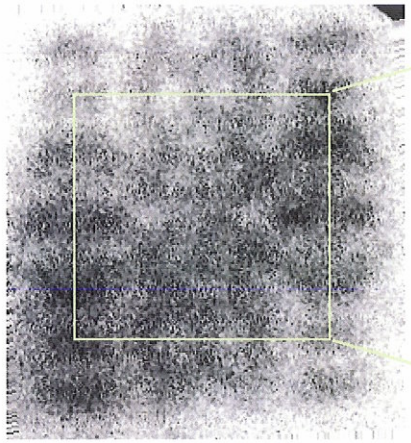

Central 300 μm - filtered after mode 6, 4 quadrants averaged

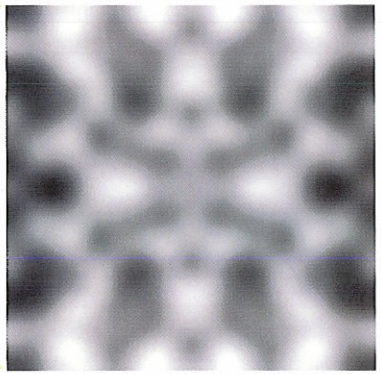

300 μm

Designed pattern

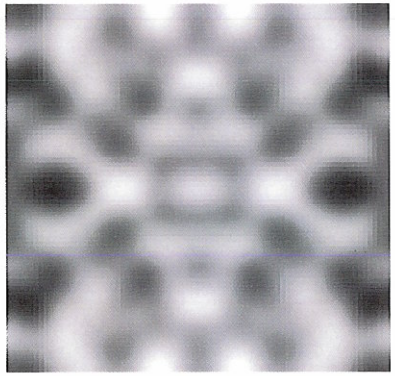

- The pattern built had an rms of ~ 0.6 μm, reflective symmetry about the center, and symmetry boundary conditions (300 μm sq

Pattern created with laser ablation of 400 Gaussian pits within each 300 μm square of $C_{50}H_{47}Br_{2.7}$ foil

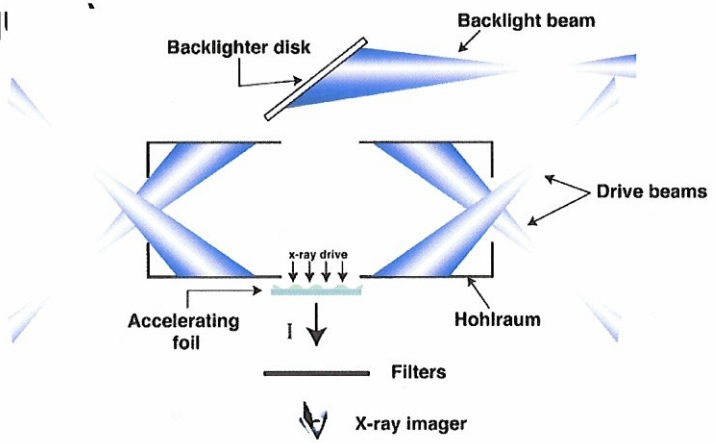

Experimental setup of foil experiment with face on radiography

HYDRA correctly simulates the features of the 3-dimensional pattern

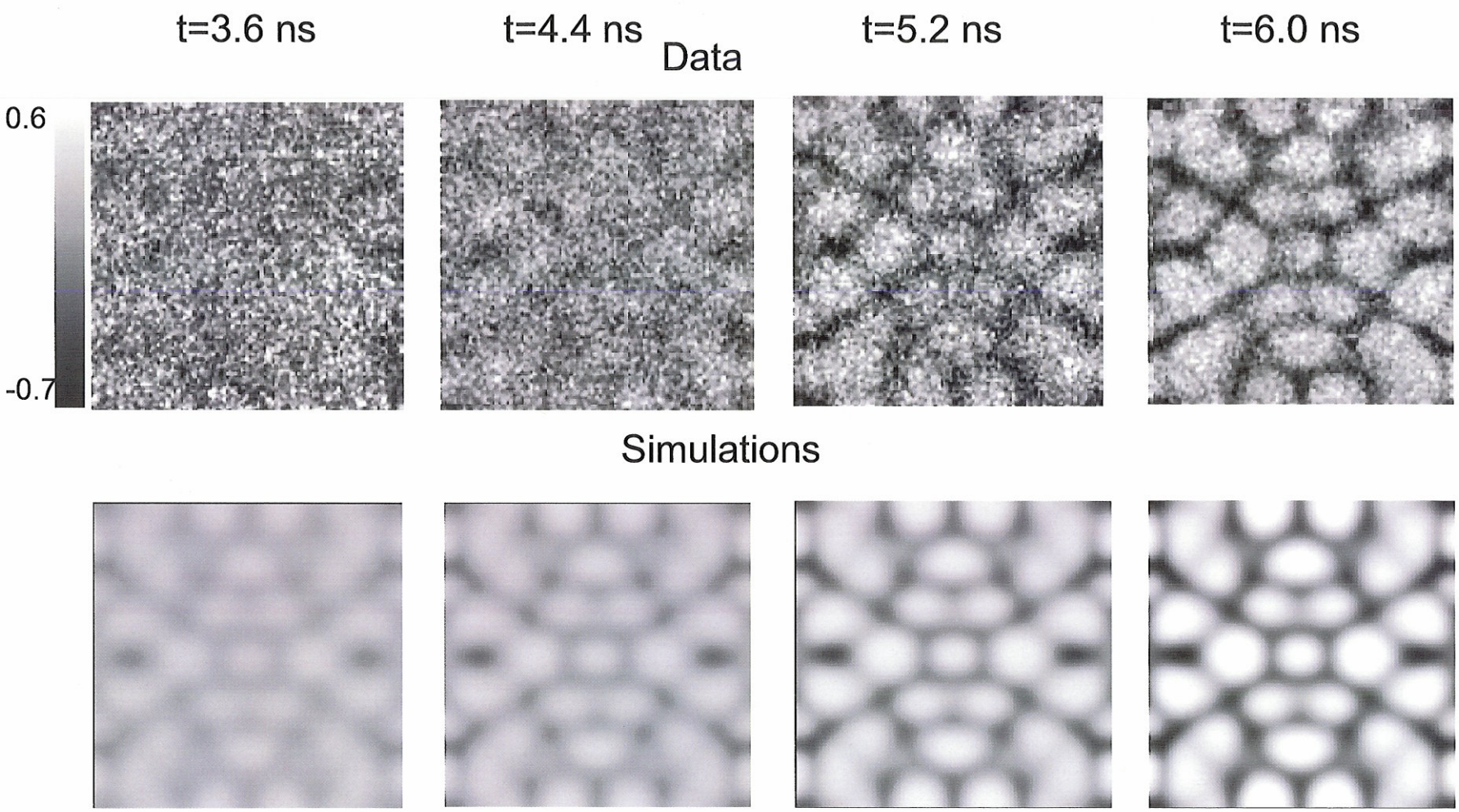

M.M. Marinak et al., Phys. Rev. Lett., **80**, 4426 (1998)

Simulated and measured RMS amplitudes are a more quantitative measure of prediction

RMS Fourier amplitude vs. mode number

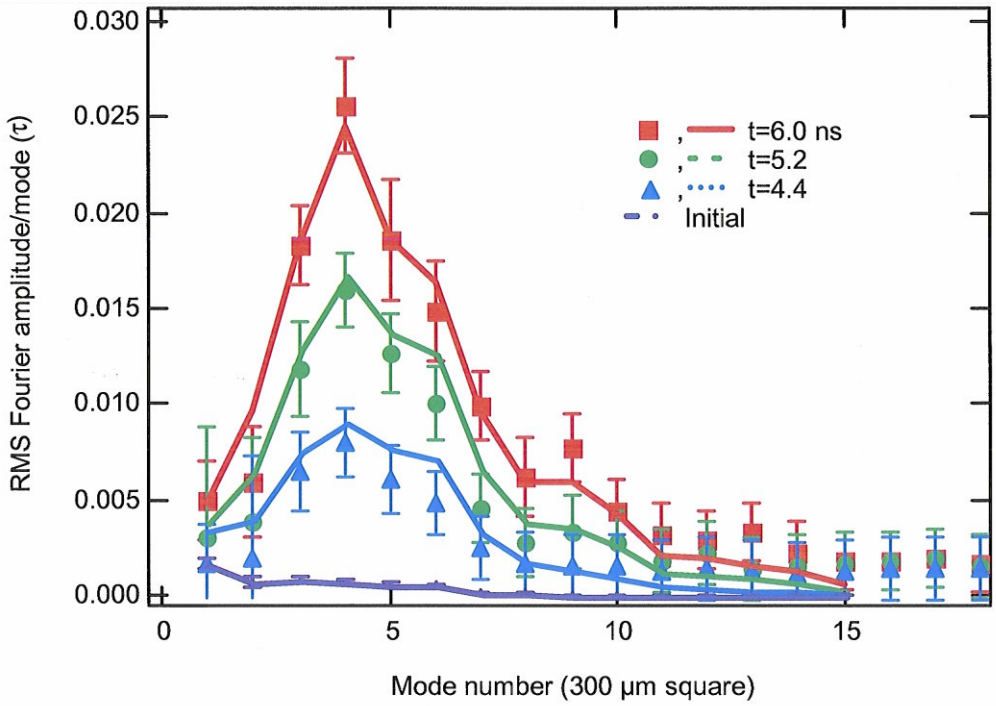

- **Spectrum is dominated by fastest growing modes**
- **Error bars on data include statistical variation of 4 images, uncertainty in fit to remove backlighter structure and the noise level of 0.0015/mode**

M.M. Marinak et al., Phys. Rev. Lett., **80**, 4426 (1998)

An experiment on Z studied perturbations arising from the presence of fill tubes on capsules

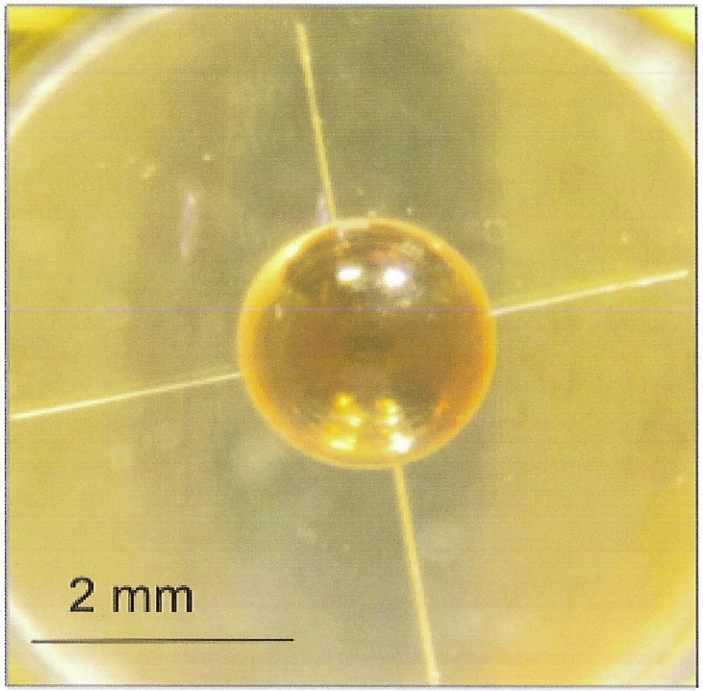

Optical image of CH capsule with 4 fill tubes (12-45 micron OD) attached around an equator

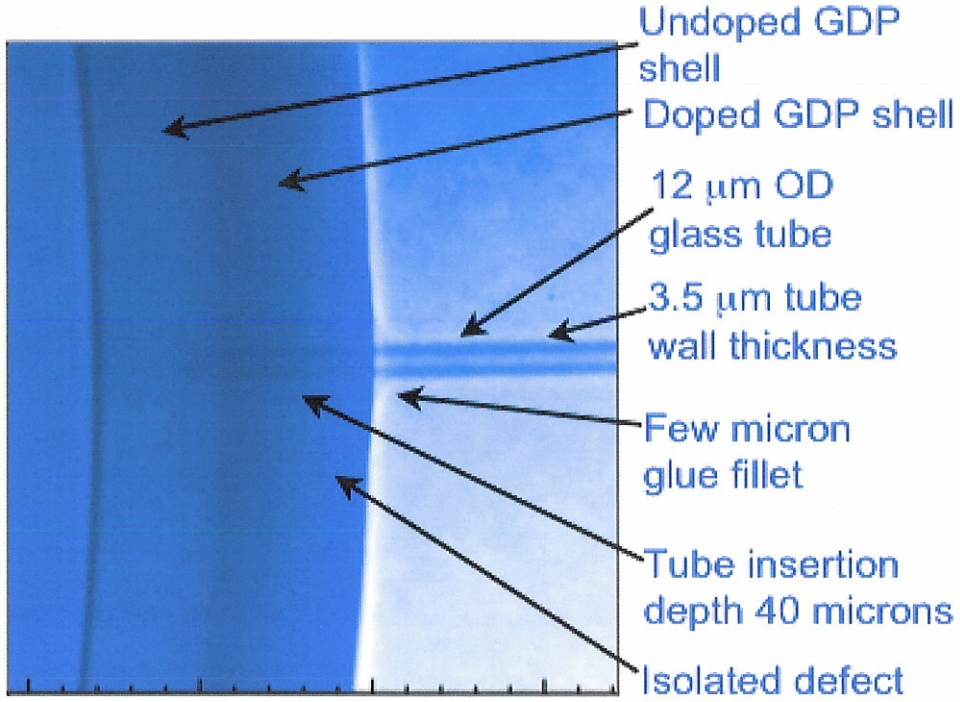

High resolution Xradia image of as built configuration gives important details for simulation

Courtesy Mark Herrmann, Sandia National Laboratory
G. Bennett et al., Phys. Rev. Lett. 99, 205003 (2007)

High resolution x-radiograph diagnostic enabled detailed comparison with contours of simulated image

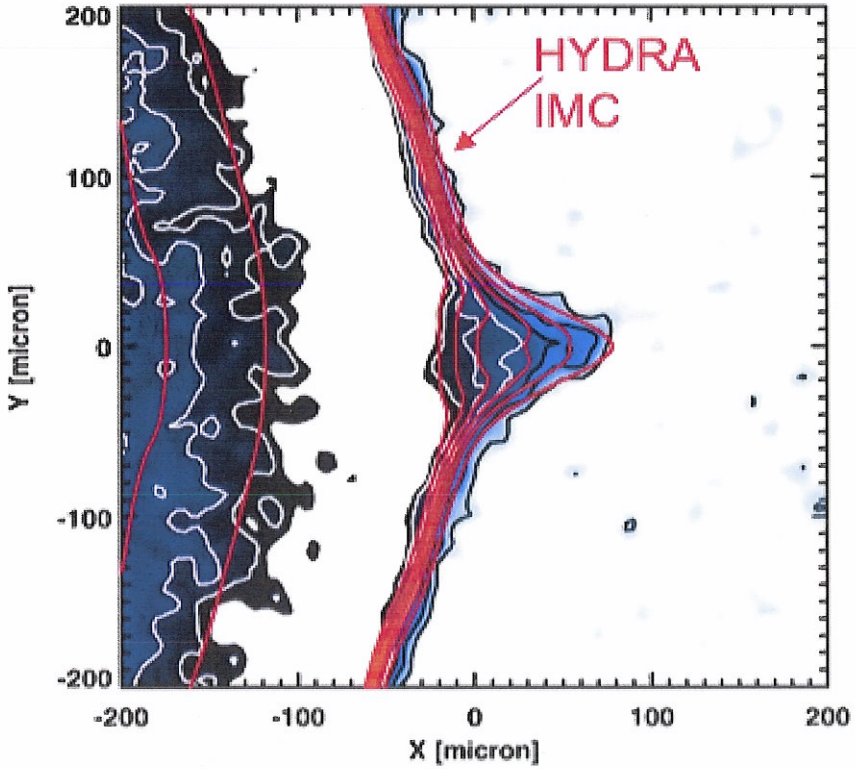

Tube D - 45 micron OD
CR = 1.55

Good agreement with experiments obtained with HYDRA simulations run using IMC radiation transport and radiation diffusion

For the largest tube (45 μm diameter) IMC yielded a better match to the data

The smaller tubes show a smaller discrepancy between IMC and multigroup diffusion

Courtesy Mark Herrmann, Sandia National Laboratory
G. Bennett et al., Phys. Rev. Lett. 99, 205003 (2007)

Monte Carlo Burn/Particle Transport enables simulation of full set of NIF particle diagnostics

- National Ignition Campaign
  - Neutron Time of Flight
    - burn temperature
    - neutron yield
  - Magnetic Recoil (MRS)
    - ρR
  - Gamma Ray Histories (GRH)
    - bang time
  - Neutron Imaging

- Improved physics: knock ons, nuclear reactions, etc.

NIF Diagnostics

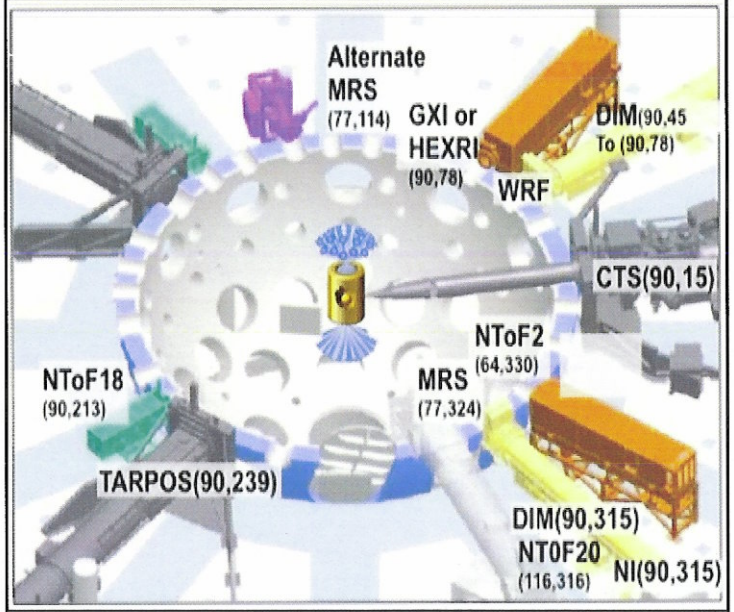

HYDRA can model the full set of NIF particle diagnostics

We examine the neutron signature of a NIF ignition capsule implosion having severe surface roughness

Surface roughness includes a 2 micron peak to valley thickness variation in ablator
Neutron diagnostics are primarily sensitive to low mode asymmetries with $\ell <= 3$

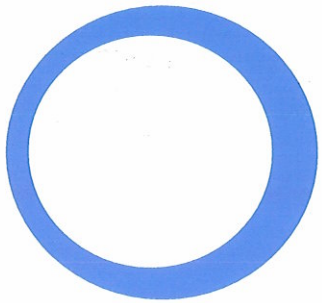

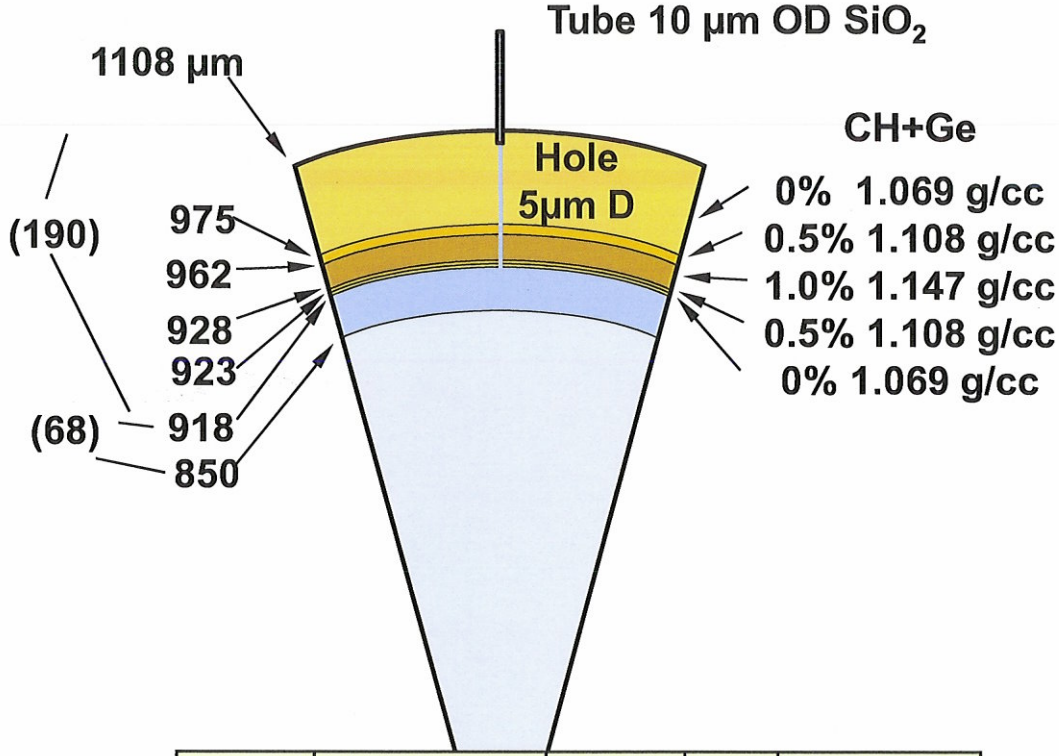

Fuel	ρ	D at%	T	^1H
Solid	0.255 g/cc	50	50	0
Gas	0.3 mg/cc	57	38	1.8

Full capsule only simulation (4π) includes intrinsic drive asymmetry and severe surface roughness

Intrinsic drive asymmetry obtained from 3D HYDRA integrated hohlraum simulation

Simulation includes roughnesses on ice and ablator surfaces through intermediate modes (ℓ <= 120), including 2 μm peak-to-valley P1

Roughness initialized on inner ice surface taken from NIF specification scaled by 0.5

Roughness initialized on ablator in range ℓ > 10 were 72 nm rms, ~ 8x NIF specification

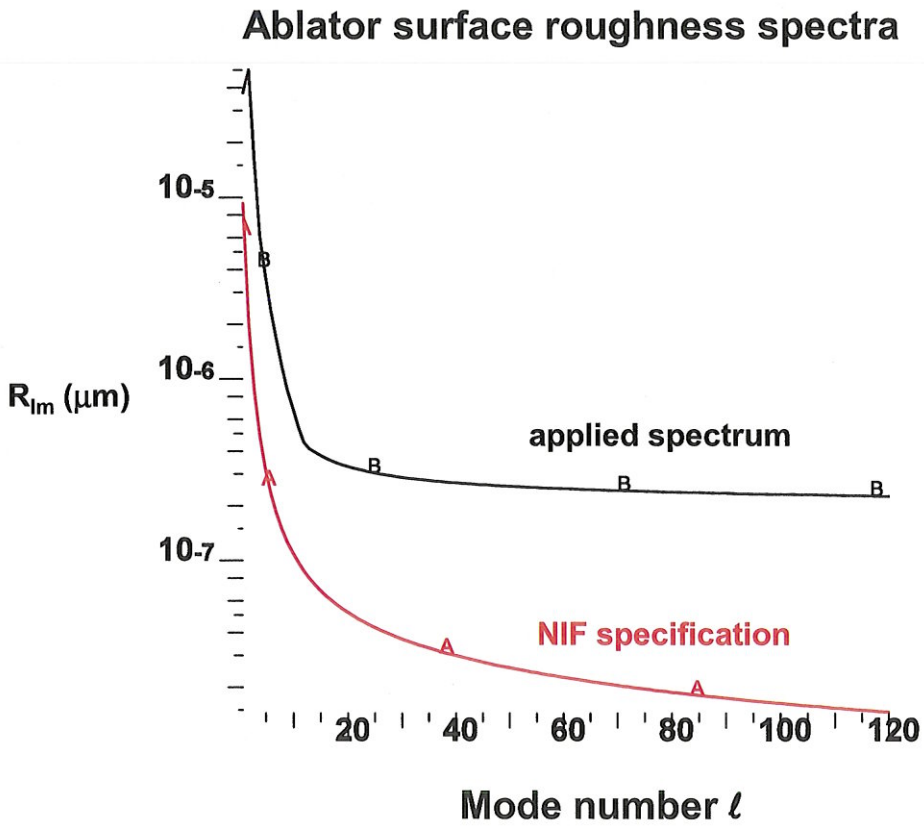

Severe perturbation applied in intermediate modes on ablator

Ablator bubbles penetrate shell before peak implosion velocity is obtained

Full 3D capsule simulation transporting neutrons, charged particles and gamma rays

57.9 million zones
run on 4096 processors

Surface roughness modes initialized using full set of spherical harmonics through $\ell = 120$

115 million particles transported at peak

Cut away view of density 2.0 g/cm^3 contour in capsule shell at 20.18 ns

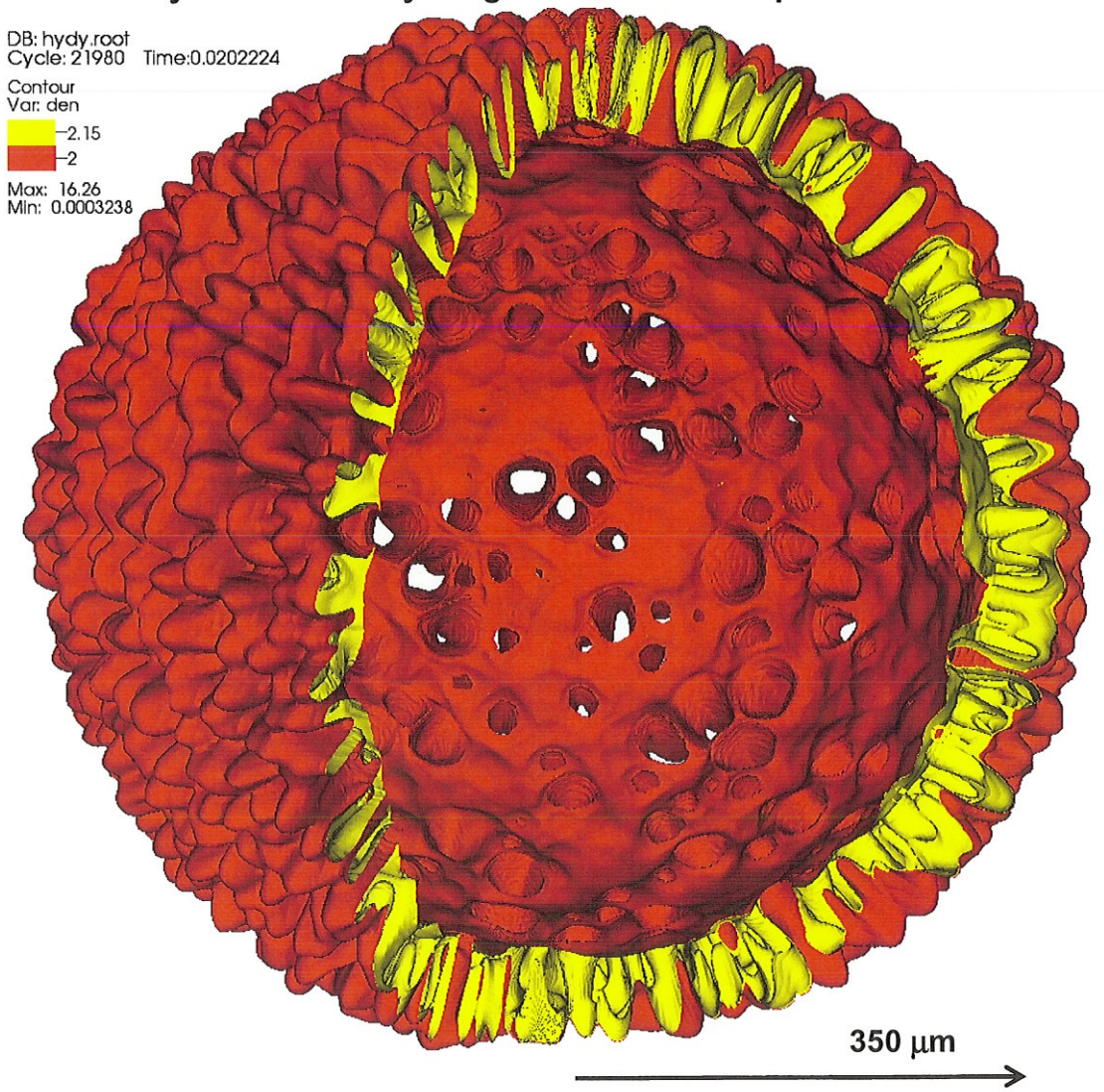

Hot spot assembly strongly perturbed by high mode RT compromising shell during implosion phase

Cut away view of density 12 g/cm^3 contour in capsule shell at 20.90 ns

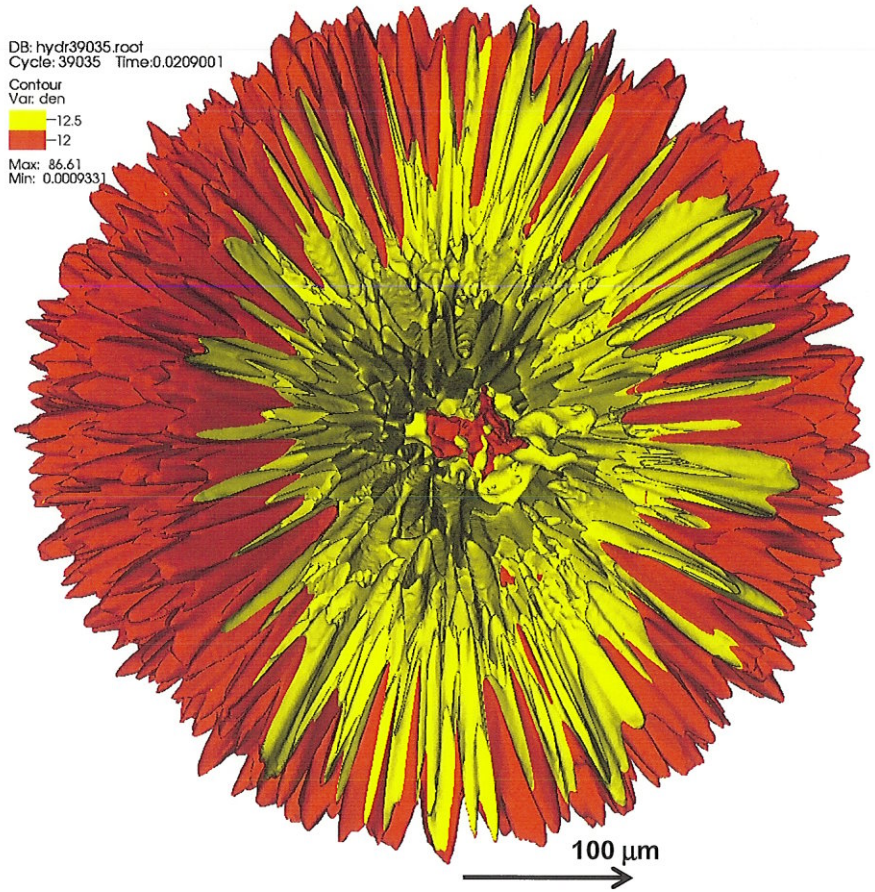

Contours in equatorial plane at 20.75 ns

Material boundaries

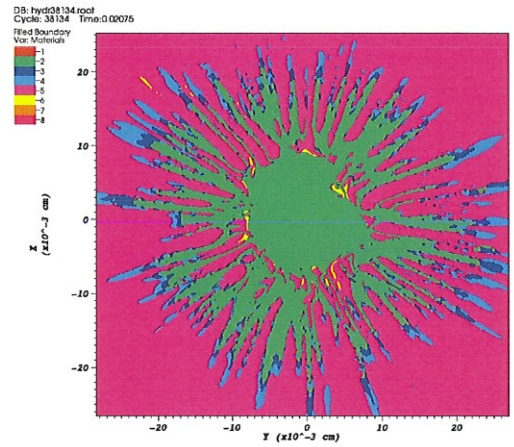

Ion temperature (keV)

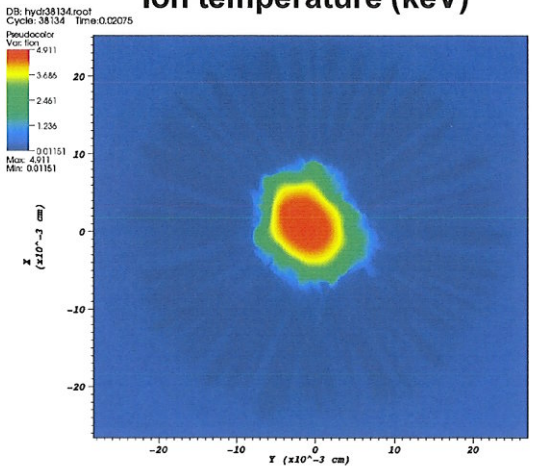

- Primary neutron yield 1.26x10^{14}
- Downscattered neutron fraction average 0.0272 average range 0.02 – 0.034
- Burn weighted ion temperature 1.22 keV

Various neutron diagnostics clearly show P1 asymmetry even with severe mix

Neutrons clearly show hot spot velocity is Doppler shifted by 30 km/s
Direction of Doppler shift correlates with orientation of P1 initial ablator thickness variation

P1 also visible in downscattered fraction

Large spectral shape distortion relative to a Gaussian (w=0.84). Indicates burn occurred over unusually broad range of temperatures.

FWHM burn temperature directional variation 1.08 to 1.40 keV (7 parameter fit) indicating significant non-spherical velocity (ℓ=2)

P1 asymmetry would be detectable with ~12 detectors scattered around solid angle measuring primary yield as long as relative measurement accuracy good to (+/- 3 %)

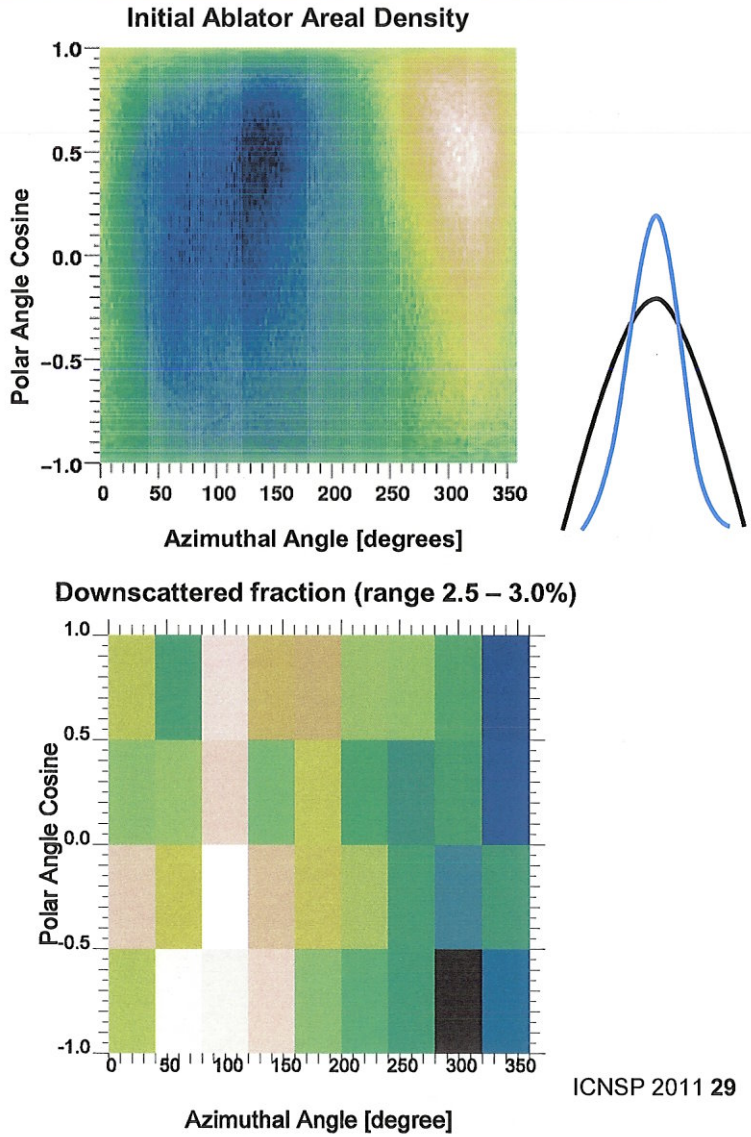

High resolution integrated simulations with HYDRA enable capsule surface perturbations to be included directly

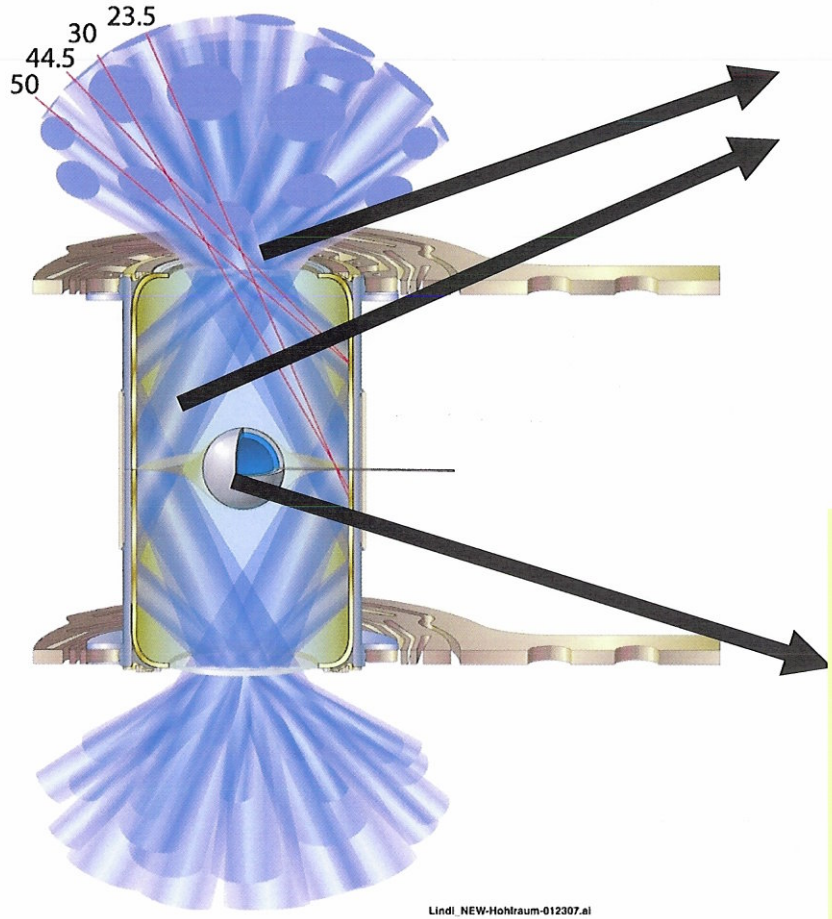

Drive and Symmetry
Inputs: Laser power, cross-beam transfer, backscatter, high-flux model
Outputs: Dante, GXD

Capsule Performance
Inputs: Drive and symmetry, capsule parameters (EOS, opacity, roughness), ice parameters (mixture, roughness), gas mixture (including deep mix)
Outputs: Neutron and x-ray diagnostics

Here we apply the technique to a THD target shot on NIF

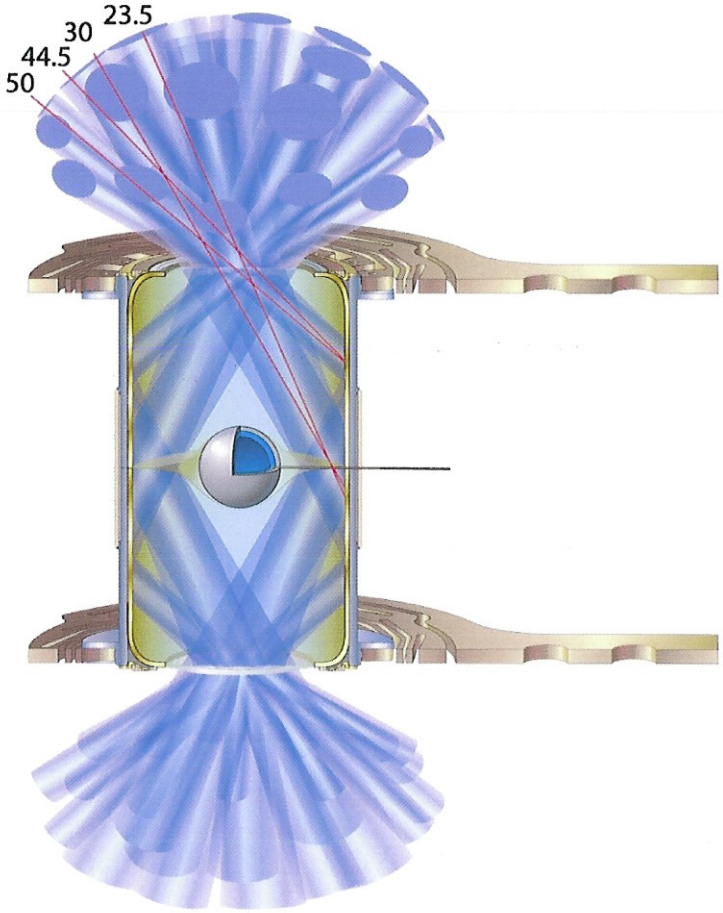

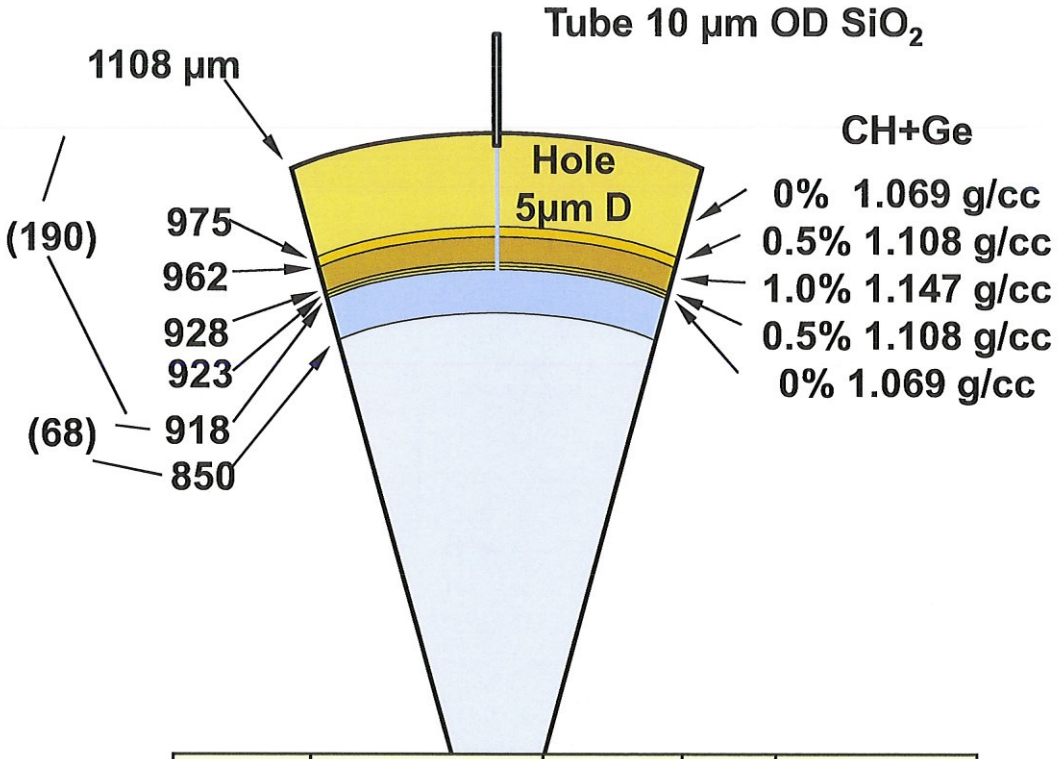

Fuel	ρ	D at%	T	^1H
Solid	0.255 g/cc	50	50	0
Gas	0.3 mg/cc	57	38	1.8

We show a time sequence of core density slices from two calculations of the THD shot

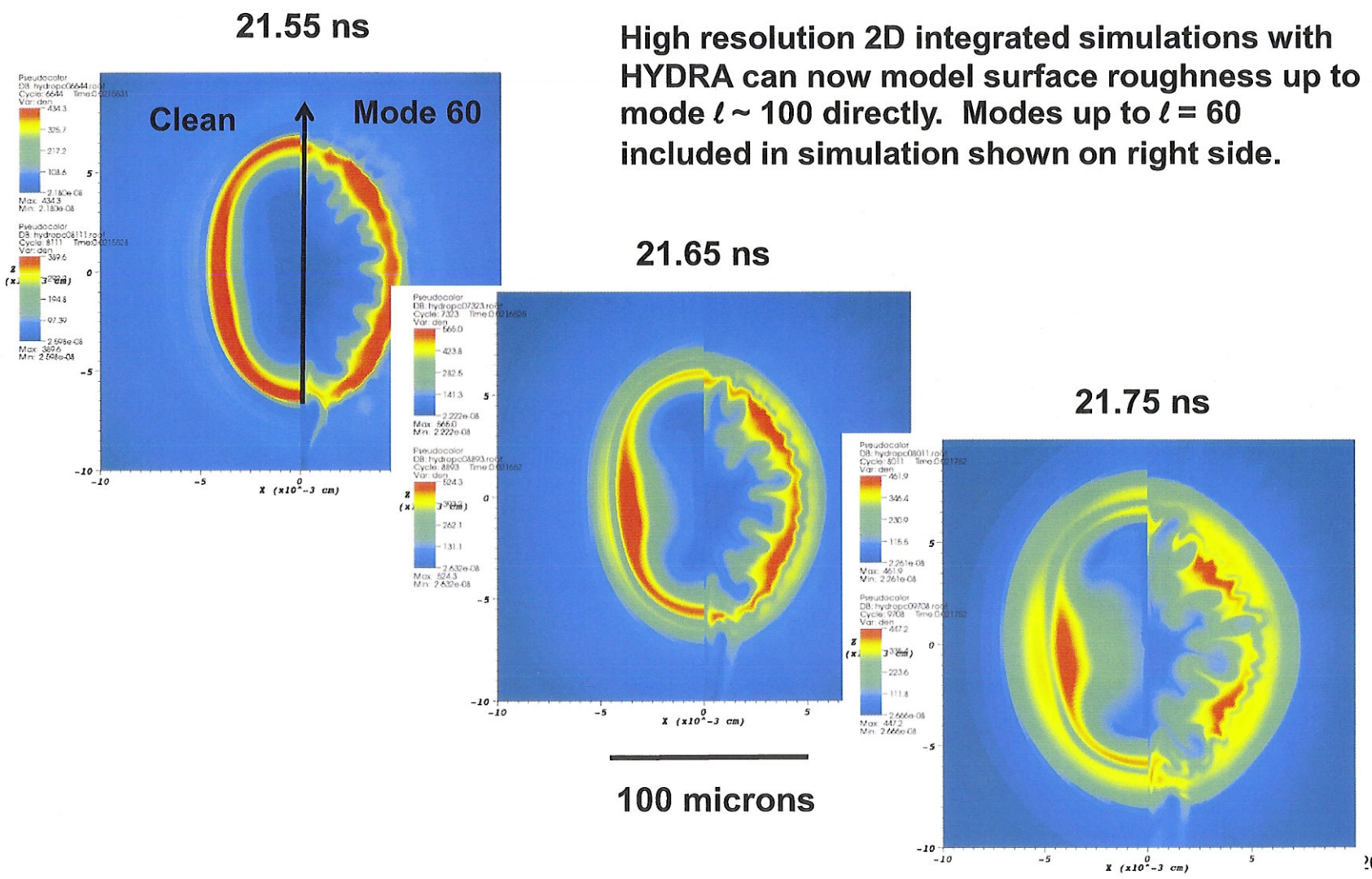

High resolution 2D integrated simulations with HYDRA can now model surface roughness up to mode $\ell \sim 100$ directly. Modes up to $\ell = 60$ included in simulation shown on right side.

A new polar S_N deterministic method for radiation transport is available in HYDRA

- Polar S_N converges with second order accuracy without significant ray effects
- Should enable more accurate treatment of fill tube calculations, radiation transport in hohlraums
- Development in collaboration with CASC (Center for Applied Scientific Computing)
- Presently runs on meshes of orthogonal quadrilaterals (2D)

Polar Sn offers higher accuracy through its novel formulation for discretizing the transport equation along a ray

$$\frac{d\psi}{ds} = q - \sigma\psi + \int_{S^2} \sigma(\vec{\Omega}\cdot\vec{\Omega}')\psi d\vec{\Omega}'$$

Polar S_N maintains exact spherical symmetry in test problems

S_N radiation transport

Capsule with fill tube provides stringent test of polar S_N transport method's convergence

Consider the shadow initially cast by a 12.5 μm diameter fill tube on baseline plastic igntion target design

Fill tube initially covers just 0.00072% of capsule surface

The tube's extremely small diameter and discontinuous opacity jump at the start provide the most challenging conditions to calculate

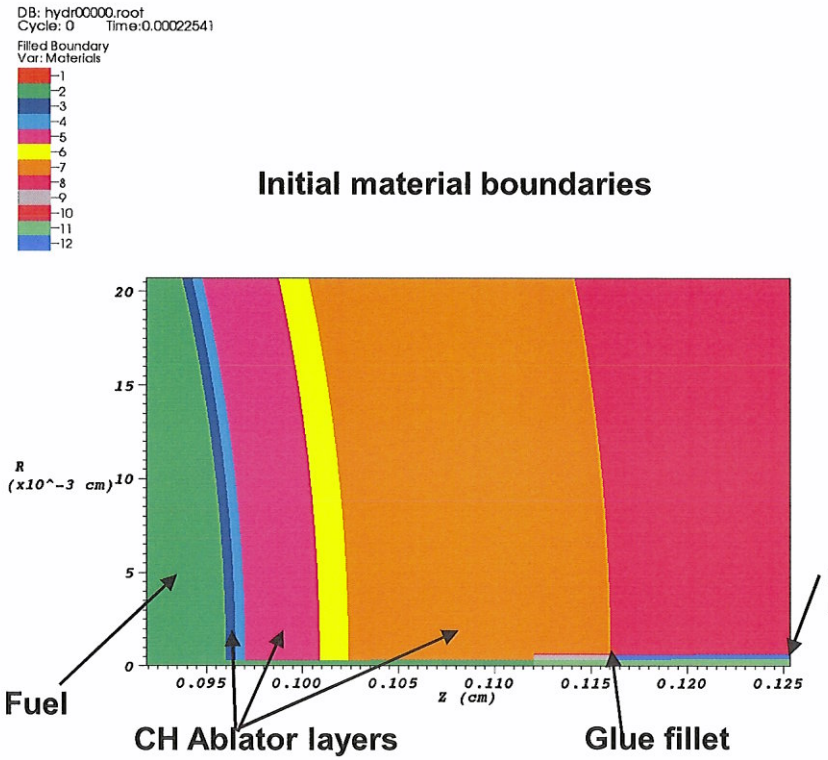

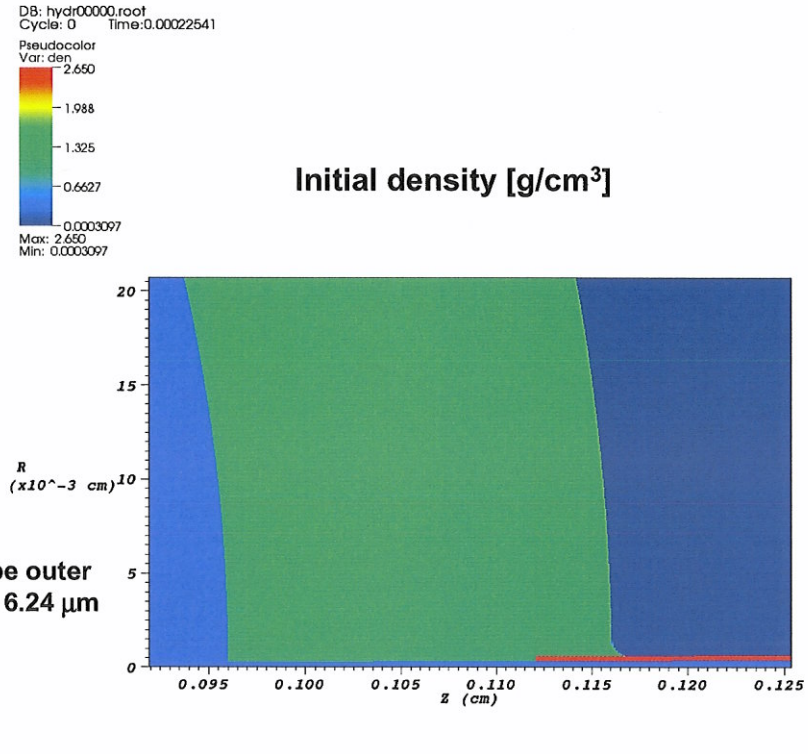

Radiation energy density on capsule surface agrees well with analytic solution for fill tube problem

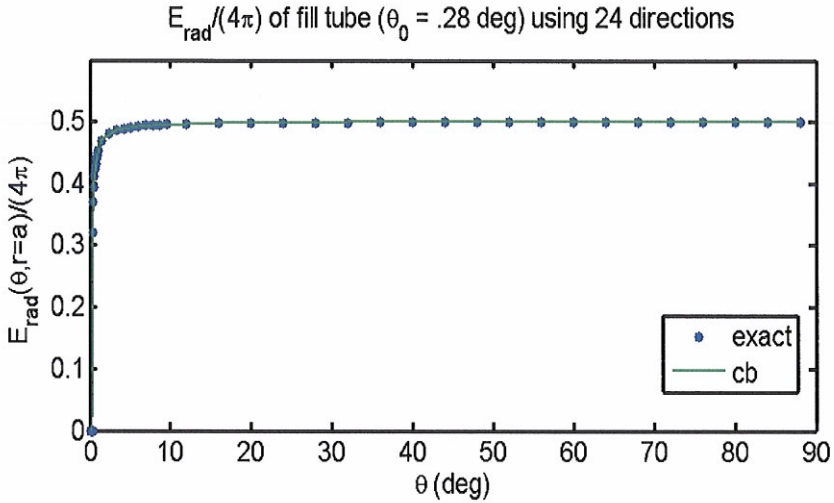

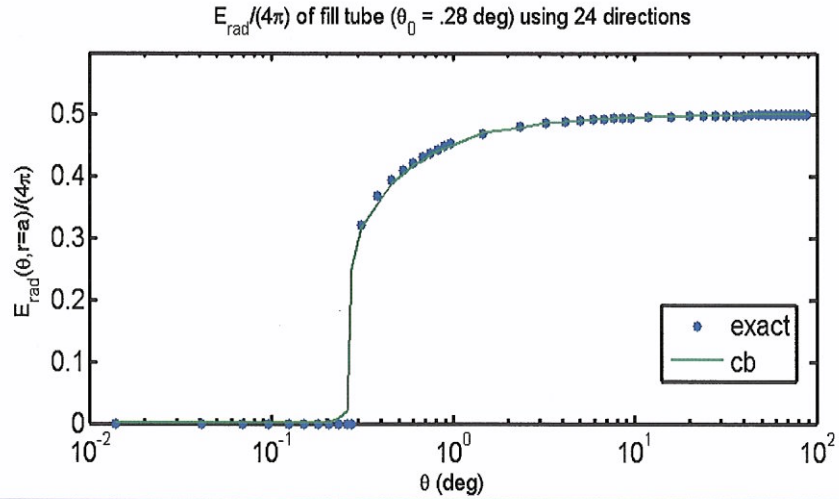

Used 6 azimuthal and 4 polar ray directions

Extent of fill tube shadow correctly modelled using 24 ray directions

Comparison of implosion simulations of NIF capsule with fill tube show excellent correspondence in weakly nonlinear phase

Density Profiles at 17.66 ns

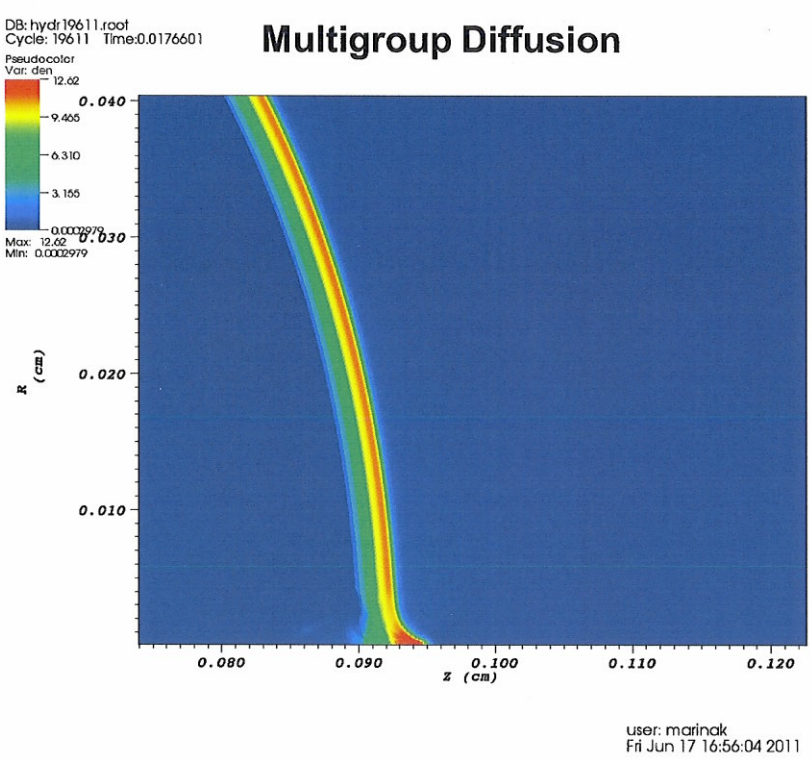

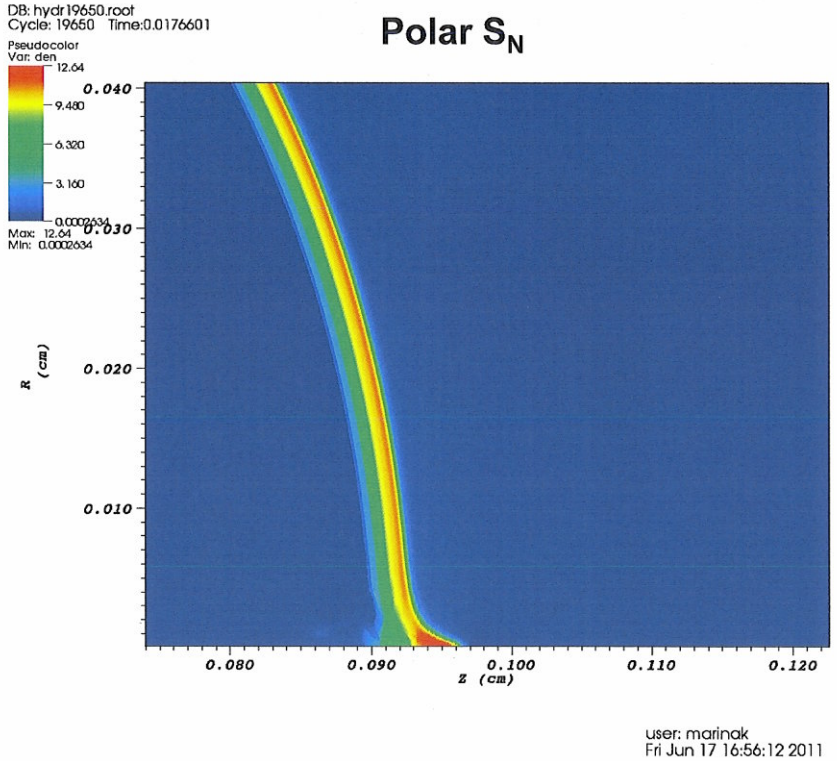

Calculations run with 60 energy groups
Polar S_N run with 24 angles -- solve and store 1440 variables per cell
Simulation domain is half a quadrant

Highly nonlinear perturbation generated by spike eventually attains larger amplitude with polar S_N transport

Density profiles at 20.6 ns

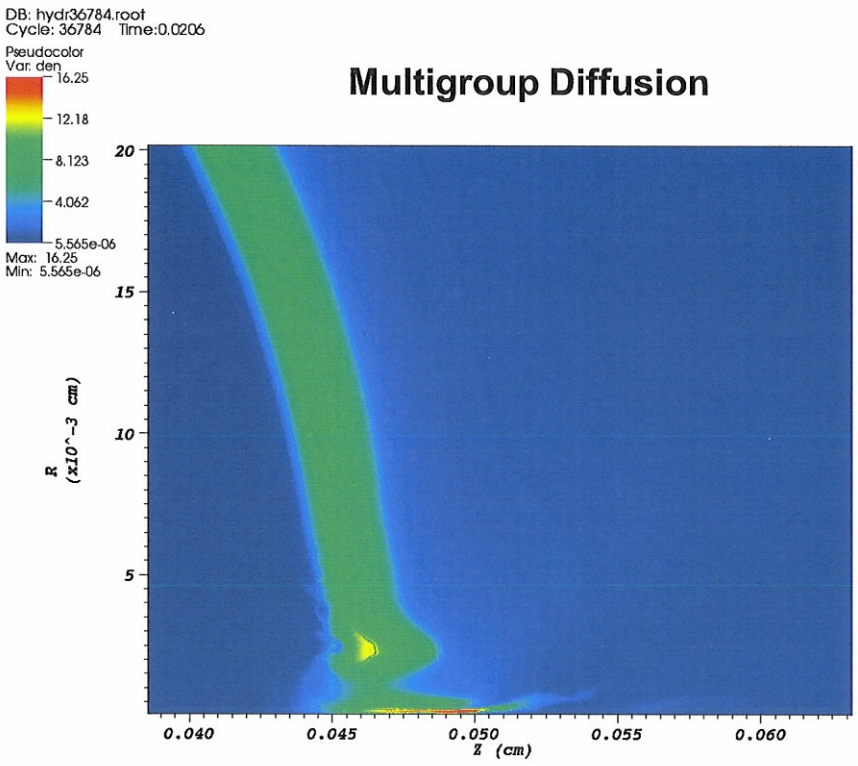

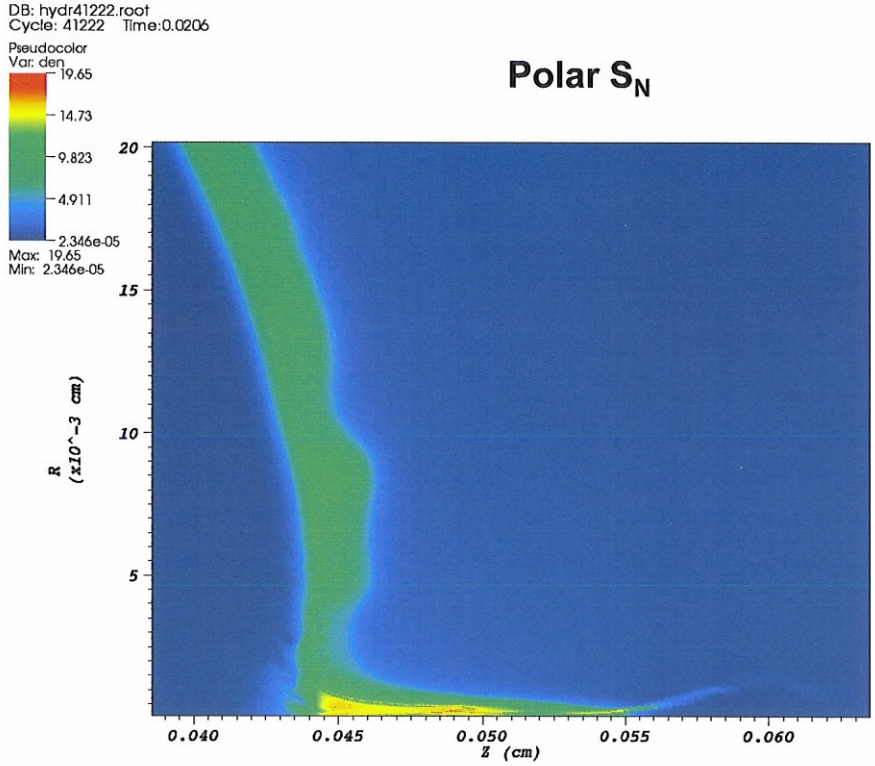

Larger amplitude is consistent with effect of self-shielding
This is treated more accurately with polar S_N

Energy transfer between crossed laser beams can now be treated with an inline model in HYDRA

- Energy transfer occurs when the beat frequency between crossed laser beam nearly satisfies the resonance condition

$$\omega_0 - \omega_1 = \left|k_0 - k_1\right| c_s + \left(k_0 - k_1\right) \cdot V$$

- We have implemented a linear model[1] for energy transfer in HYDRA's 3D laser raytracing package
- Cross beam energy transfer equations can be written in the form

$$\frac{\partial}{\partial \tau_1} I_1 = C_{12} I_1 I_2$$

$$\frac{\partial}{\partial \tau_2} I_2 = C_{21} I_1 I_2$$

- Coupling coefficients C_{12}, C_{21} require evaluations of the electron and ion susceptibilities χ_e, χ_i with respect to beat ion accoustic wave

1. P. Michel et. Al, Phys. Plasmas **17**, 056305 (2010)

Cross beam laser energy transfer

When integrated along the rays the overall energy conservation equations are obtained

In terms of the ray powers for rays (r_1,r_2) in beams (b_1,b_2) the equations can be expressed as

$$\frac{\partial}{\partial \tau_1}\sum_{r1}\overline{P}_{r1}\tau_{r1}\,|_{b2} = C_{12}\sum_{r1}\overline{P}_{r1}\tau_{r1}\sum_{r2}\overline{P}_{r2}\tau_{r2}\,/\,\Delta V$$

$$\frac{\partial}{\partial \tau_2}\sum_{r1}\overline{P}_{r2}\tau_{r2}\,|_{b1} = C_{21}\sum_{r1}\overline{P}_{r1}\tau_{r1}\sum_{r2}\overline{P}_{r2}\tau_{r2}\,/\,\Delta V$$

Integrating along a single ray across a zone we get the power transfer relation

$$\delta\overline{P}_{r1} = \sum_{q} C_{1q}\overline{P}_{r1}\tau_{r1}I_q$$

The cross beam transfers for beams (b_1,b_2) are related by

$$\frac{\sum_{r1}\delta\overline{P}_{r1}\,|_2}{\sum_{r2}\delta\overline{P}_{r2}\,|_1} = \frac{C_{12}}{C_{21}} = -\frac{\lambda_2^{\,v}}{\lambda_1^{\,v}} = -\frac{\omega_1}{\omega_2}$$

The balance of energy goes into the ion accoustic beat wave

$$\Delta P^{ia} = \Delta P_{12} + \Delta P_{21} = \Delta P_{12}(1-\frac{\omega_2}{\omega_1})$$

Ray transport equations are iterated to obtain a self-consistent solution

- Iterative solution is required since the cross beam transfer itself depends upon the intensity
- On the nth iteration, we adjust the zonal ray power depletion due to inverse bremsstrahlung to include the cross beam coupling by

$$\nu_{r1}^{n} \equiv \frac{\partial \ln I_1}{\partial \tau}\Big|_{bq} \longrightarrow \nu_{ibr1} - \sum_q C_{1q} I_q^{n-1} = \nu_{ibr1} - \sum_q \nu_{1q}^{n-1}$$

Zonal intensities are recalculated during each iteration by accumulating the contributions for each ray in each beam including the cross beam coupling

Obtain excellent energy conservation, usually convergening to ~ 10^{-6} in 4-5 iterations

An empirical saturation limit is applied to the density wave amplitude

- Density wave amplitude driven by each beam pair interaction is limited by a user-specified value

$$\left|\frac{\delta n_e}{n_e}\right|_{q,q'} \equiv S_t$$

Using

$$\left|\frac{\delta n_e}{n_e}\right|_{q,q'} \equiv C^{n_e}_{q,q'}\sqrt{I_q I_{q'}}$$

we obtain

$$v_{qq'} \equiv \frac{\partial \ln \delta\overline{P}_{rq}\,|_{q'}}{\partial \tau} = \min(C^{n_e}_{qq'}\sqrt{I_q I_{q'}}, S_t) C^{Q}_{qq'}\sqrt{I_{q'}/I_q}$$

Effects of cross beam transfer illustrated in simplified test problem

- 4 laser cones each consisting of 6 lasers with angles (23.5°, 30°, 44.5°, 50°) rotated at 15° in azimuth relative to each other
- Propagates through H at 0.1 keV, 1 x 10^{-4} g/cm^3 extending from z = (-0.5, 0.5) cm
- Plasma is at rest
- In linear regime results from inline model and post-processed result agree well

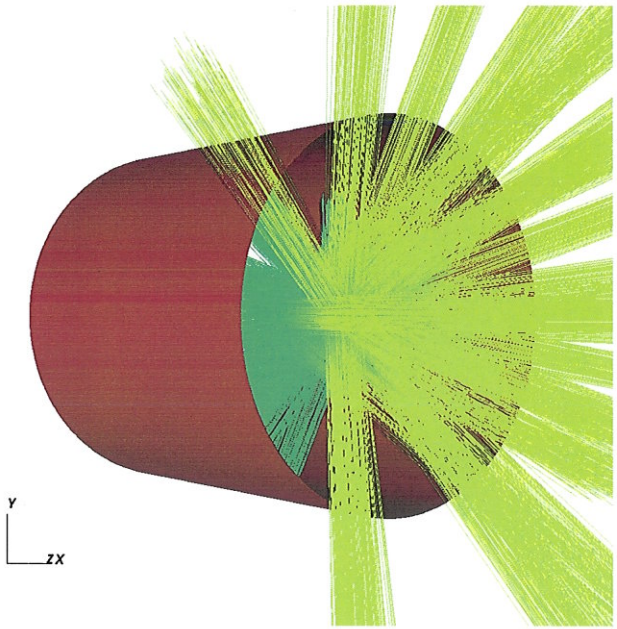

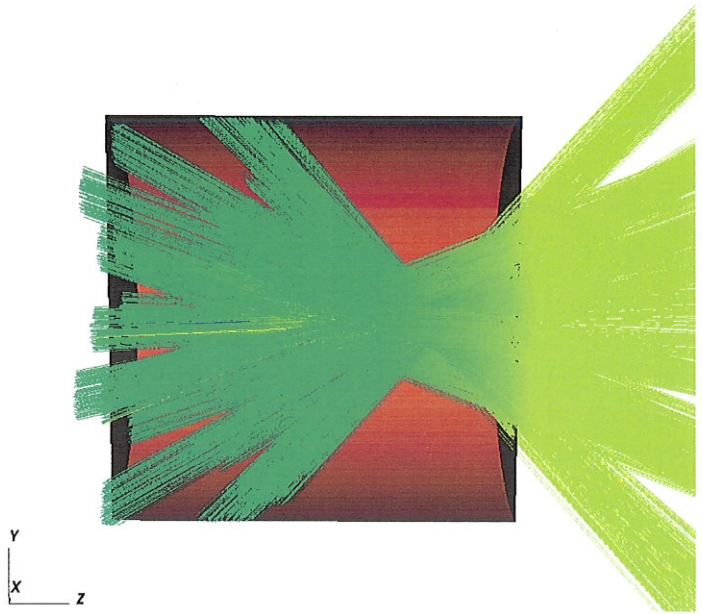

User:
Fri Nc

Cross beam transfer alters the laser spot profile as well as average intensity

Downstream of the interaction region, where the beams overlapped, the cross beam transfer has exchanged power between the beams and modified the laser spot profiles

Net change in laser intensity due to cross beam transfer at a plane beyond locations of beam overlap

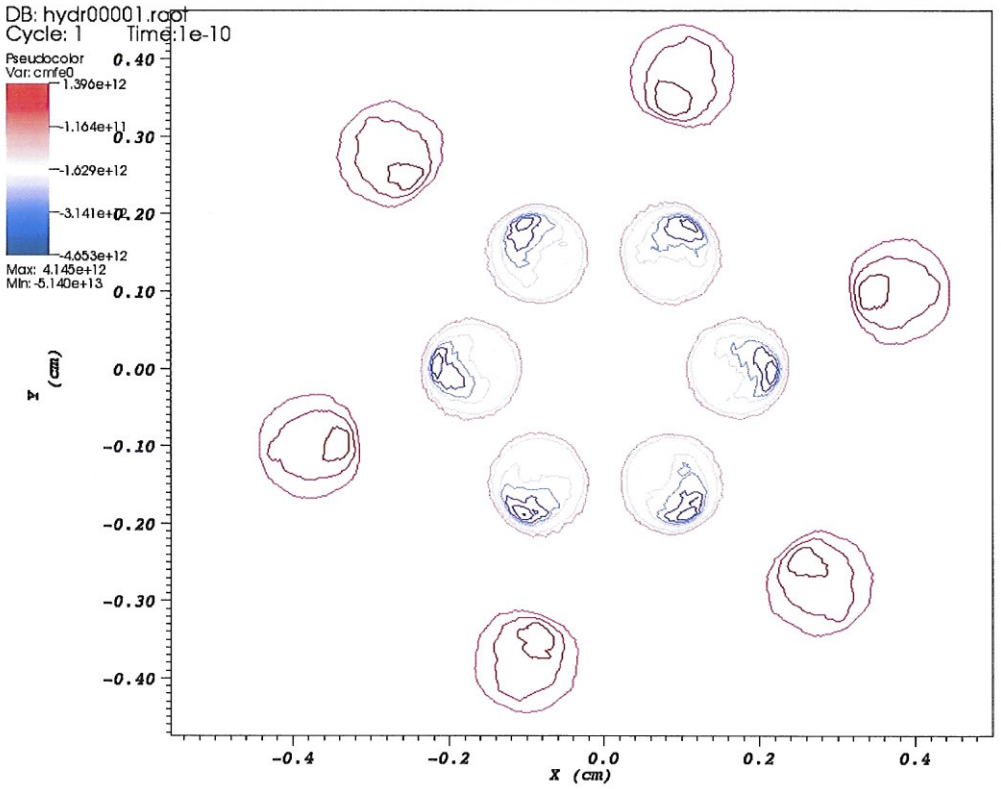

We apply the inline cross beam transfer model to a 3D integrated simulation of a THD shot

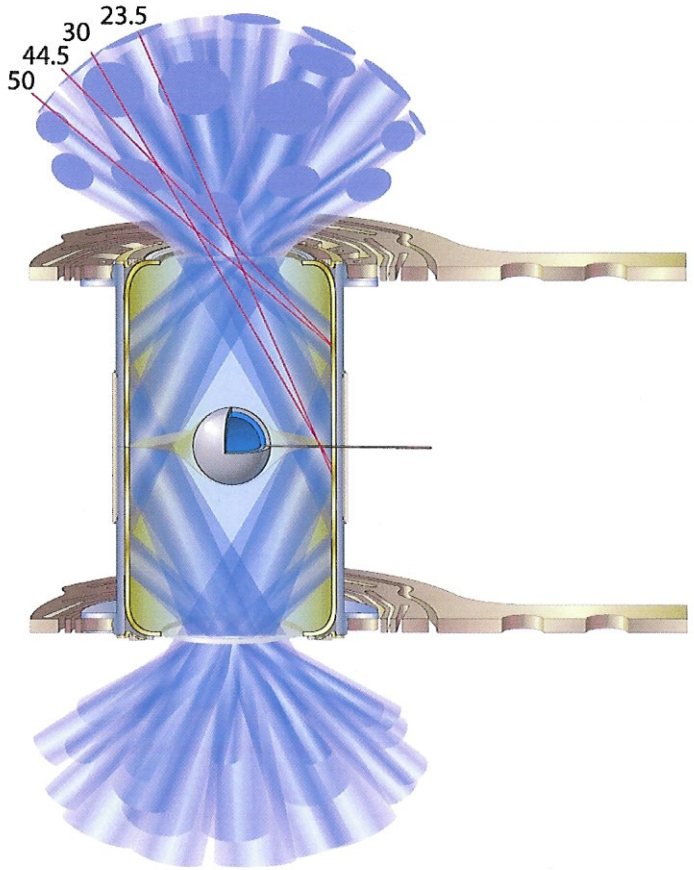

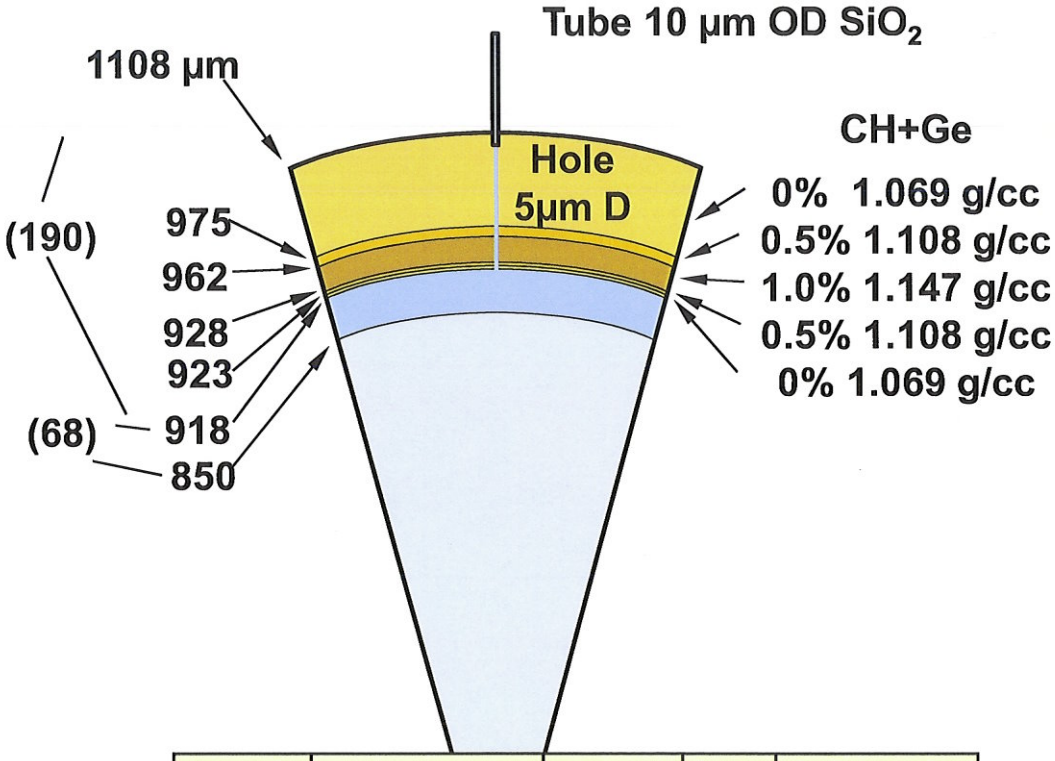

Fuel	ρ	D at%	T	^{1}H
Solid	0.255 g/cc	6	72	22
Gas	0.3 mg/cc	0.7	7.3	92

"3 color" configuration with 23.5° beam offset by 2A. 23.5° beam wavelength 10527.5 A, all others 10525.5 A

Cross beam laser energy transfer

We compare power transfer between cones obtained with two methods

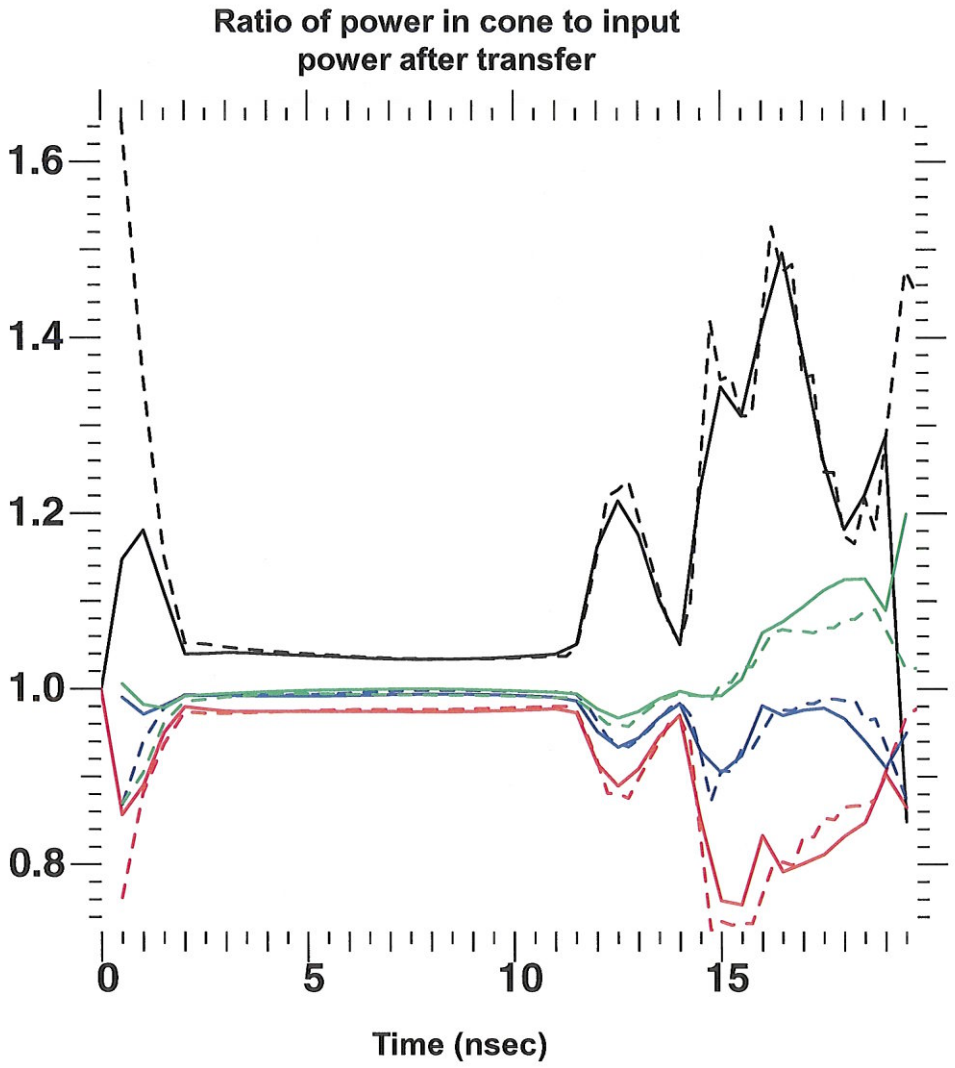

- 23.5° cone inline
- 30° cone inline
- 44.5° cone inline
- 50° cone inline
- 23.5° cone post process
- 30° cone post process
- 44.5° cone post process
- 50° cone post process

Cross beam transfer with applied saturation limit parameter 6×10^{-4}

Ponderomotive force included in simulation

Disagreement between models before 2 ns stems from effects of laser burn through not accounted for in post processed model

Inline model accounts for beam refraction, plasma conditions and beam overlap self-consistently

HYDRA runs on a wide variety of platforms

- HYDRA can run in a distributed parallel mode and is fully scaleable
- Massively parallel ASC and WCI platforms, consisting of clustered SMP architectures
- State of the art parallel techniques implemented in a portable manner
  - POSIX threads, OpenMP and the MPI message passing libraries
  - Dynamic load balancing achieves efficient operation for the IMC and laser libraries
  - Domain replication implemented to avoid strong scaling limit
- Simulations run on as many as 65536 processors
- Simulations with over 100 million zones have been run

We are modifying HYDRA to enable it to make effective use of Sequoia

- We have implemented the capability to do domain replication in IMC to avoid a strong scaling limit
  - High resolution 3D hohlraum including surface roughness
- We expect Sequoia will enable very high resolution capsule only simulations over large solid angle
  - Recent 2.5° wedge resolved up to $\ell \sim 1200$ in 3D. Used 67 million zones - run on 4096 processors
  - Using full 1.5 million cores on Sequoia might enable ~100 x greater solid angle at this resolution
- One important application for parallel computing is 1D and 2D parameter scans comprising thousands run simultaneously
- In anticipation of exascale computing platforms we are investigating practicality of running on GPUs
  - Presently investigating how IMC package could be run on LLNL Edge machine (GPUs)

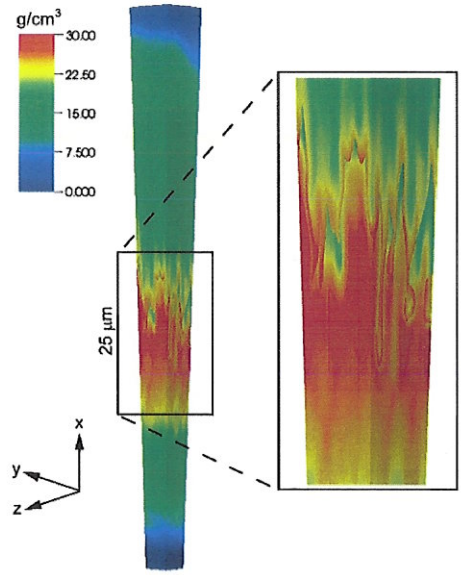

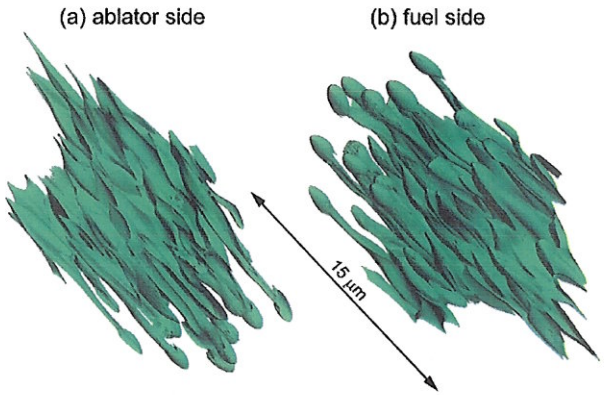

Radiation hydrodynamics simulation with inline treatment of parametric instabilities has long been a goal

- HYDRA has inline models for SBS and SRS
  - Allow user to specify what fraction of energy is backscattered, at specified density with specified redshift (SRS)
- LPI simulation resolves 3D wave structure of parametric instabilities as well as ponderomotive filamentation
- PF3D uses paraxial approximation
  - Spatial scale resolved to 1.25 λ zones in transverse direction, 2-8 λ in axial for f8 speckles
  - Temporal scale of simulation steps set by light transit time across cell
  - Simulation of single beam requires 5 x 10^{10} zones run on 16000 processors for 14-28 days to complete several hundred time periods
- HYDRA integrated simulation – zoning near laser entrance hole ~100 μm, temporal scale several psec per step
  - Full target integrated simulation runs on 1024 processors for ~1-2 days

Inline calculation of LPI

- Consider a simulation with perfect power balance and pointing.
- Could link from hydro code to LPI code, overlaying plasma fields onto fine mesh
- Run LPI simulation of beam for required number of global light transit times to quasi-steady state
- Backscattered fraction, beam spray conveyed to 3D laser raytrace through differential scattering cross section
- Calculation performed for one beam from each of 23.5, 30, 44.5, 50 degree cones
- Power deposition in rad hydro code then adjusts for backscatter, beam spray using scattering coefficient
- HYDRA and PF3D could exchange data using existing inline linker

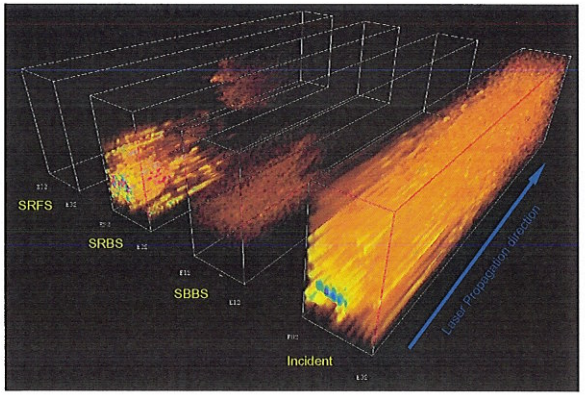

This approach may become practical in the not too distant future

Conclusions

HYDRA is a versatile ICF design code used to model a broad variety of targets

- Ongoing development in HYDRA is enabling increasingly accurate treatment of complex physics
- Wide range of physical models available for designer to choose
- Broad variety of model ingredients supported for EOS, opacities, conductivities, …
- HYDRA has been tested extensively against data on NIF, Omega, Nova, Titan, with a long list of results published in refereed journals
- We've tested ability to model every aspect of hydrodynamic instability physics important in NIF capsule implosions
- Extensive diagnostics on many shots provide stringent tests of our models
- High resolution integrated simulations enable capsule surface roughness to be included directly